https://doi.org/10.5194/egusphere-2025-974
Preprint. Discussion started: 21 March 2025

Multitemporal analysis of Sentinel-1 backscattering during snow melt using high-resolution field measurements and radiative transfer modeling

Francesca Carletti[1], Carlo Marin[2], Chiara Ghielmini[1], Mathias Bavay[1], and Michael Lehning[1,3]

[1]WSL Institute for Snow and Avalanche Research SLF, Davos, Switzerland
[2]Institute for Earth Observation, Eurac Research, Bolzano, Italy
[3]School of Architecture, Civil and Environmental Engineering, École Polytechnique Fédérale de Lausanne EPFL, Lausanne, Switzerland

Correspondence: Francesca Carletti (francesca.carletti@slf.ch)

Abstract. The spatiotemporal evolution of snow melt is fundamental for water resources management and risk mitigation in mountain catchments. Synthetic Aperture Radar (SAR) images acquired by satellite systems such as Sentinel-1 (S1) are promising for monitoring wet snow due to their high sensitivity to liquid water content (LWC) and ability to provide spatially distributed data at a high temporal resolutions. While recent studies have successfully linked S1 backscattering to various phases of snowpack melting, a correlation with detailed snowpack properties is still missing. To address this, we collected the first dataset of detailed wet snow properties tailored for SAR applications over two consecutive snow seasons at the Weissfluhjoch field site in Switzerland. First, our dataset enabled the validation of previous methods relying on multitemporal SAR backscattering to characterize melting snowpacks and physically linked the increase in backscattering following the local minimum to the evolution of surface roughness. Then, the dataset was used as input to the Snow Microwave Radiative Transfer (SMRT) model to reproduce the S1 backscattering signal. Our simulations showed a general negative bias compared to the satellite data, with the most significant drivers being LWC early in the melt season and the surface roughness later on. The results also highlight several key challenges for reconciling S1 signals with radiative transfer simulations of wet snow: (i) the discrepancy in spatiotemporal variability of LWC as seen by the satellite and validation measurements, (ii) the lack of fully validated permittivity, microstructure and roughness models for wet snow in the C-band, (iii) the difficulty of capturing wet snow features potentially generating stronger scattering effects on a large scale, such as internal snowpack structures, soil features in case of low LWC, and surface roughness, which are not necessarily captured by point-wise measurements.

1 Introduction

Seasonal snowpack in mountain catchments is one of the most important water resources, as it accumulates and stores water during winter and releases it consistently in the form of runoff during the melting period (Viviroli and Weingartner, 2004). In fact, discharge in Alpine streams is largely dominated by snow melt from May to July and more than one sixth of the world's population relies on meltwater released from higher altitudes for drinking water, crop irrigation and hydropower production (Beniston et al., 2018). However, this melting snow can also cause wet- and glide-snow avalanches (Bellaire et al., 2017; Fromm

https://doi.org/10.5194/egusphere-2025-974
Preprint. Discussion started: 21 March 2025

et al., 2018), which pose significant threats to human life and infrastructures. Additionally, rain-on-snow events on snowpacks with high liquid water content are linked to increased runoff and shorter time lags between the onset of the event and the resulting runoff (Würzer et al., 2016). These events can have catastrophic consequences and their occurrence is supposed to increase as a first response to sustained warming (Beniston and Stoffel, 2016). Therefore, information about the spatiotemporal evolution of snow melt is beneficial for the management of water resources and for risk mitigation.

Identifying wet snow is complex both when using manual measurements, automatic instruments and physically based snow models. Datasets of manual measurements of snow water equivalent (SWE) and liquid water content (LWC) at high temporal resolution are generally rare due to the required amount of work and resources to collect them. There have been considerable advances in the development of technologies that exploit the dielectric properties of snow in the microwave range to estimate LWC in a non-destructive way (Schmid et al., 2014; Koch et al., 2014). However, the application of these methods is limited to one single point without the possibility to capture the spatial variability of the processes. Additionally, their installation and maintenance is often complicated and expensive, and the extraction of the physical parameters is usually hindered by noise. Physically based layered snow models like the SNOWPACK-Alpine3D model chain (Bartelt and Lehning, 2002; Lehning et al., 2006) or GEOtop (Endrizzi et al., 2014) are used to overcome these challenges, as they can simulate LWC and SWE at high spatial and temporal resolutions only based on meteorological forcings. However, meteorological forcings also represent a major source of uncertainty - especially when needed at high spatial resolution - affecting the accuracy of the results (Raleigh et al., 2015), together with the uncertainty related to the amount and type of used parametrizations (Günther et al., 2019).

In this context, a valuable opportunity to identify wet snow is offered by synthetic aperture radar (SAR) systems. SAR measurements are highly sensitive to the free liquid water contained in wet snow (Nagler and Rott, 2000). At certain frequencies, the increase in liquid water generates high dielectric losses and increased absorption coefficients (Denoth et al., 1984; Sihvola and Tiuri, 1986; Mätzler, 1987; Ulaby et al., 2014). Therefore, the radar backscattering drops to lower intensities with respect to winter averages (Ulaby et al., 1987, 2014; Nagler and Rott, 2000; Nagler et al., 2016; Lin et al., 2016). Basing on this principle, multitemporal SAR data were used to develop algorithms for the generation of wet-snow maps (Nagler and Rott, 2000; Nagler et al., 2016). There have been further efforts in developing algorithms to derive LWC using C-band full-polarimetric SAR images (Shi et al., 1993; Shi and Dozier, 1995). However, Strozzi et al. (1997); Kendra et al. (1998) expressed their doubts about the theoretical background and the systematic reliability of these algorithms. With tower-based experiments on wet snow, they found that the backscattering behavior used for the retrieval algorithms might have been biased by a combination of conditions leading to a strong prevalence of surface scattering mechanisms.

After a progress freeze due to the lack of SAR data in the past and simultaneous ground truth measurements, there was a renewed interest in the use of radar waves to track snow melting processes since the launch of the Sentinel-1 (S1 hereafter) joint mission of the European Space Agency (ESA) and the European Commission in 2014. At Alpine latitudes, S1 acquires C-band SAR imagery in the early morning and late afternoon, regardless of the weather, with a revisit time of 6 days. The SAR imagery is available free of charge. Marin et al. (2020) used these images for the first time to develop a correlation between the multitemporal S1 SAR backscattering and the snowmelt dynamics. Over 5 different Alpine sites, the authors have found that the multitemporal S1 SAR acquisitions allow the detection of the melting phases, i.e. moistening, ripening and runoff

https://doi.org/10.5194/egusphere-2025-974
Preprint. Discussion started: 21 March 2025

(Dingman, 2015) with a good agreement with in-situ observations and layered, physically-based snow models. In particular, the backscattering decreased as soon as liquid water appeared in the snowpack and increased progressively and simultaneously with the runoff release. Deriving and applying a set of identification rules, the authors could define the melting phases for the test sites with relatively small lag errors with respect to the revisit time of S1.

This approach holds great potential for monitoring the temporal evolution of melting dynamics, especially over wide and scarcely instrumented areas. However, in order to fully understand the potential of the multitemporal information made available from S1 for snowmelt monitoring, a deeper understanding of the scattering mechanisms of melting snow is needed. In particular, knowing the time window in which different scattering effects dominate and under which conditions the the C-band radar backscattering is fully absorbed by the melting snowpack would enable to extract as much information as possible from S1 multitemporal backscattering. Up-to-date, the only effort in this direction has been done by Brangers et al. (2024) by means of tower-based C-band measurements, which, however, lack ground-truth validation at high temporal resolution with measured snow properties. Additionally, the snowpack melt-out has been often associated with sharp increases in backscattering following the local minima (Marin et al., 2020; Darychuk et al., 2023; Gagliano et al., 2023). However, the underlying physical processes that determine this trend, among which the effect of surface roughness (Marin et al., 2020), remain to be investigated.

The main limitation that has hindered the understanding of SAR mechanisms is the lack of reference ground data, especially during the melting season. Over Alpine snowpacks, it is not uncommon to observe the formation of ice layers either at the surface (Quéno et al., 2018) or at deeper snowpack depths (Pfeffer and Humphrey, 1998). Moreover, in temperate Alpine areas characterized by high snow accumulation and intense solar radiation, suncups may form spontaneously on the snow surface during the ablation season (Post and LaChapelle, 2000; Mitchell and Tiedje, 2010), increasing the surface roughness significantly (Fassnacht et al., 2009). These phenomena are known to impact the radar response to wet snow (Kendra et al., 1998; Yueh et al., 2009; Nagler and Rott, 2000; Shi and Dozier, 1995).

A promising path to explore the interaction between C-band active microwaves and scattering properties of wet snow surfaces is through state-of-the-art radiative transfer (RT) models. Picard et al. (2018) developed the Snow Microwave Radiative Transfer (SMRT) model, a versatile model that can be used in active and passive mode to compute backscattering and brightness temperature from multilayered media such as snowpacks or ice sheets overlying reflective surfaces e.g. ground, ice, or water. SMRT responds to the need of a modular and flexible approach to unify and compare the wide range of pre-existing representations of microstructure, electromagnetic theories, soil models and permittivity formulations. While wet snow holds significant importance for various applications, both SMRT and other similar models have primarily been developed and validated under dry snow conditions in Arctic and Antarctic snowpacks, or ice sheets (Proksch et al., 2015; Rott et al., 2021; Soriot et al., 2022; Meloche et al., 2022; Husman et al., 2023). Both the vertical structure and the surface of these types of snowpack are often less complex than that of a seasonal Alpine snowpack. To date, the above mentioned ensemble of complex melting snowpack processes has been scarcely investigated by means of radiative transfer models due to the lack of ground reference data (Shi and Dozier, 1995; Strozzi et al., 1997; Kendra et al., 1998; Nagler and Rott, 2000; Magagi and Bernier, 2003; Lodigiani et al., 2025). Murfitt et al. (2024) recently used SMRT to explore, for the first time, the temporal evolution of

https://doi.org/10.5194/egusphere-2025-974
Preprint. Discussion started: 21 March 2025

the interaction between wet snow and radar waves in a study on lake ice melt. However, the radiative transfer modeling of wet snow still lacks dedicated effort and validation.

This work aims at collecting the first ground reference dataset on melting snow for SAR applications and to verify the ability of a current, state-of-the-art RT model (SMRT) to reproduce the backscattering signal recorded by S1. Previously, only Lund et al. (2022) carried out an extensive snow pit campaign in coordination with S1 passages. Their work facilitated the interpretation of S1 backscattering response to diurnal snowpack features. However, important scattering properties such as the optical diameter and the surface roughness were not sampled and their effect on the backscattering was not explored through radiative transfer modeling. In this work, we focus on the co-polarized vertical backscattering only, due to its high signal to noise ratio for wet snow (Naderpour et al., 2022) and to the fact that, due to the partial implementation of some of the key processes, it is not possible to simulate accurate cross-polarized backscattering responses with the current version of SMRT. To our knowledge, this is the first attempt to use SMRT and ground measurements specifically designed for RT modeling – including wetness and roughness – to reproduce S1 backscattering over a wet, multilayered Alpine snowpack. This research will allow us to derive several important information on RT modelling of wet snow, namely the influence of the spatial and temporal variability of liquid water content within the S1 cell occurring between satellite acquisitions and in situ measurements, the influence of surface roughness, the lack of fully validated models of permittivity and roughness for wet snow at the C-band and the difficulty of capturing key wet snow conditions generating scattering, namely internal snowpack structures, large-scale surface roughness, interactions with the wet soil interface when the snowpack is only slightly wet. With ground reference data and adequate process understanding and modeling, RT models like SMRT may evolve in tools to interpret and translate the information contained in multitemporal SAR backscattering signals into valuable input for snow modeling.

2 Campaign overview

This work builds upon a dataset composed of 85 snow pits collected within a measurement campaign which took place over the two consecutive snow seasons of 2022-2023 and 2023-2024 at the high-altitude field site of Weissfluhjoch Versuchsfeld (WFJ), located in the Rhaetian Alps in the Davos area, canton of Grisons, Switzerland. The measurement field lies at an altitude of 2536 m a.s.l. on a relatively flat area embedded in a valley facing south-east. The site is partially wind sheltered from a small hill situated on the south-east, however the dominant wind blows from north-west in addition to katabatic wind. For this measurement campaign, we secured a protected field covering approximately the same footprint area of S1, i.e. 20×20 m next to the officially delimited field. However, only a fraction of this field was effectively used for measurements. This designated area has a light slope value between 2 and 7%. The flatness of the terrain is fundamental for the study of the interaction between wet snow and the C-band co-polarized vertical backscattering signal (σ_0^{VV} hereafter). On the one hand, σ_0^{VV} is less sensitive to changes in snow wetness in areas of steep topographies (Nagler et al., 2016); on the other hand, steep slopes cause the liquid water to redistribute laterally, at least partially (Wever et al., 2016). The field site of WFJ is equipped with advanced meteorological sensors recording meteorological forcings at sub-hourly resolutions, and moreover, with first snow observations dating back to 1936, it holds one of the longest recorded time series of snow measurements for a high-altitude research station

https://doi.org/10.5194/egusphere-2025-974
Preprint. Discussion started: 21 March 2025

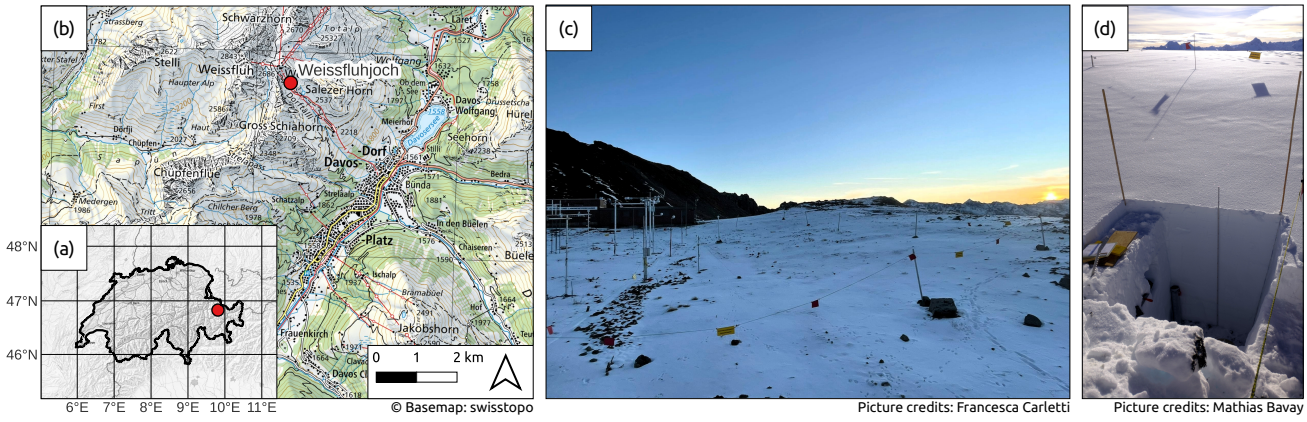

Figure 1. Location of the Weissfluhjoch field site with respect to Swiss national borders (a) and the area of Davos (b). The area dedicated to the snow profiles is shown in (c), delimited by the flagged fence, camera facing north-east. Only a fraction of the length of the fenced area was effectively used for snow profiles. Picture (d) shows the typical snowpit measurement setting.

(Marty and Meister, 2012). The site is ideal for intensive measurement campaigns, as it is easily accessible, protected from avalanche danger and the two huts provide shelter, storage space for instruments, power and internet connection.

The objective of the measurement campaign was to build a dataset that would provide ground-truth reference for the interpretation of S1 σ_0^{VV} to monitor snow melt processes. Therefore, the campaign targeted the main scattering properties of snow: temperature, density, specific surface area (SSA), liquid water content (LWC) and surface roughness. These properties needed to be measured at a high vertical and temporal resolution to track the progression of the wetting front within the snowpack, and possibly in concomitance with S1 acquisitions. Additionally, we measured snow water equivalent (SWE), a key variable for snow melt monitoring. The resulting dataset is a time series of manually measured snow profiles describing the evolution of snow scattering properties at an unprecedented vertical and temporal resolution. The dataset consists of 38 snow profiles for the season of 2022-2023 (starting in February and ending in June) and 47 for the season of 2023-2024 (starting in November and ending in July). In dry snow conditions, measurements were carried out once per week. On the first season, once the snowpack reached the full isothermal state, measurements have been carried out regularly every second working day for a total of three times per week. On the following season, the regularity of the measurements was partially given up in favour of a better synchronization with S1 acquisitions. To get the fullest possible picture to interpret the melt dynamics, manual measurements are accompanied by automatically recorded time series of runoff and SWE.

2.1 Manual measurements

2.1.1 Temperature

Snow temperature serves to monitor the progression of the snowpack to the (partial) isothermal state, which allows the presence of liquid water. Profiles of snow temperature were sampled from the surface to the bottom with a vertical resolution of 10 cm

https://doi.org/10.5194/egusphere-2025-974
Preprint. Discussion started: 21 March 2025

on snow season 2022-2023 and of 5 cm on snow season 2023-2024 using a batch of HI98501 Checktemp from Hanna (HannaInstrumentsInc.). According to the instrument specifications, the uncertainty range is $\pm$ 0.2°C. Each temperature reading was marked down after waiting an adequate time for measurement stabilization.

2.1.2 Density

Profiles of snow density were sampled from the surface to the bottom with a vertical resolution of 3 cm using a box density cutter and a digital scale. The box cutter used for this campaign has a volume of 100 cm^3. The uncertainty range of this instrument is between 5 and 10% with the main uncertainty sources being caused by the presence of ice layers, the compaction of light snow while collecting the sample or losing fractions of the sample in conditions of fragile snow such as facets or depth hoar (Conger and McClung, 2009; Proksch et al., 2016).

2.1.3 Specific Surface Area

Profiles of snow specific surface area (SSA) were sampled from the surface to the bottom with a vertical resolution of 4 cm using the InfraSnow sensor from FPGA (FPGA Company; Wolfsperger et al., 2022). This non-destructive method builds upon the principle of diffuse near-infrared reflectance measurements using a compact integrating sphere setup to derive optical equivalent grain diameter (OED), and therefore SSA (Gergely et al., 2014). To compute OED, snow density is required as an input parameter and for this we use the measured density profile. With a relative error of $RMSE$ =15% (Wolfsperger et al., 2022) when compared to μ-CT, this instrument seems to be slightly less accurate than others commonly used such as the IceCube (Zuanon, 2013), however, this bias is more pronounced for high values of SSA typical of dry snow, which is not the main object of our study. Moreover, the use of the InfraSnow is especially practical and portable for field applications.

2.1.4 Liquid Water Content

Profiles of snow liquid water content (LWC) were sampled from the surface to the bottom with a vertical resolution of 2, 5 or 10 cm, depending on the method. We used dielectric sensors coupled with melting calorimetry to corroborate measurements in conditions of high LWC at later stages of the melting process. To our knowledge, this is the first time series of liquid water content snow profiles measured at such high vertical and temporal resolution. On the first campaign year, we used the Denoth capacitive sensor (Denoth, 1994) ("Denothmeter" hereafter). It consists of a flat capacitance probe with an estimated measurement surface of 176 cm^2 (Techel and Pielmeier, 2011). The probe operates at a frequency of 20 MHz and measures the real part of the permittivity of snow, and a separate measurement of density is required to obtain the imaginary part (Denoth et al., 1984; Denoth, 1989) – here, similarly than for SSA, we used the measured density profile. The Denothmeter has been widely used in field studies to monitor the evolution of snowpack wetness (Fierz and Föhn, 1994; Kattelmann and Dozier, 1999; Techel and Pielmeier, 2011), alone or in comparison with other techniques, e.g. in Koch et al. (2014); Wolfsperger et al. (2023); Barella et al. (2024). On the second campaign year, we adopted the new capacitive snow sensor (NCS hereafter) developed at the Institute for Snow and Avalanche Research SLF (Wolfsperger et al., 2023) and produced in batch series

https://doi.org/10.5194/egusphere-2025-974
Preprint. Discussion started: 21 March 2025

from FPGA company. The use of the Denothmeter was discontinued because it is not commercially available, and only two units were available to us, risking measurement continuity if damaged during intensive use. The NCS works in the same way as the Denothmeter, operates at the same frequency and measures over a slightly larger surface of 202 cm^2. The NCS was compared against the Denothmeter in both field and lab settings and the agreement was generally good, however, in some cases of very wet layers (Fierz, 2009), the measured permittivity tended to deviate towards higher values (Wolfsperger et al., 2023). A good element of consistency is that the comparison between the NCS and the Denothmeter was carried out within this campaign, in the snow season 2022-2023. The absolute error associated with dielectric measurements was estimated around 1% in volume (Sihvola and Tiuri, 1986; Fierz and Föhn, 1994). To our knowledge, a systematic study on the errors associated with the Denothmeter was never carried out. However, similar studies are available for the Finnish snow fork (Sihvola and Tiuri, 1986), which directly measures both real and imaginary parts of snow permittivity. The error associated to the snow fork in measuring LWC is between $\pm$0.5% (Sihvola and Tiuri, 1986) and $\pm$0.3% (Moldestad, 2005). (Techel and Pielmeier, 2011) used both the Denothmeter and the Snow Fork in their study, reporting differences of around 1% between the two instruments. Additional uncertainties for dielectric measurements derive from interference with solar radiation near the surface (Lundberg, 2008), which we tried to minimize throughout the campaign.

Because dielectric devices may lose accuracy for high LWC values (Perla and Banner, 1988; Techel and Pielmeier, 2011), for both snow seasons, in conditions of ripe snow, measurements with Denothmeter/NCS were backed up with melting calorimetry following the revised field protocol recently described in Barella et al. (2024) and partially carried out within the same measurement campaign described here. This field protocol is tailored to reduce the higher uncertainty ranges previously associated to melting calorimetry (Kawashima et al., 1998; Kinar and Pomeroy, 2015; Avanzi et al., 2016). It proposes a revised formulation of the calorimetric uncertainty that incorporates the calorimetric constant and the propagation of uncertainties coming from instrument, operational and environmental conditions. The uncertainty range associated with the new protocol for melting calorimetry is $\pm$0.5% and the absolute error compared with Denothmeter measurements is $\sim$1% in volume.

2.1.5 Surface Roughness

Snow surface roughness is typically expressed using three parameters: the root mean square of the heights (RMSH), the correlation lenght (CL) and the autocorrelation function (Williams and Gallagher, 1987; Nagler and Rott, 2000; Manninen et al., 2012; Anttila et al., 2014). These parameters can be obtained from a digitized snow transect. A proven and robust system involves inserting a panel into the snow and capturing images of the snow surface with a digital camera (Manninen et al., 2012; Anttila et al., 2014). For this campaign, we used the method described in Barella et al. (2021), which builds upon these concepts and it is particularly apt for field applications. The panel we used is made of black Forex, 70.5 cm wide and 47 cm tall. These dimensions are a trade-off between the ease of transport and the length of the snow transect covering at least 10 times the C-band wavelength λ=5.5 cm as suggested in (Manninen et al., 2012). The panel can be photographed by means of any digital camera. To attain a representative snow transect, 9 pictures were taken on each campaign day: 3 along one direction, 3 along the perpendicular direction, and 3 at a 45° angle between them. The resulting roughness profile is averaged among all

https://doi.org/10.5194/egusphere-2025-974
Preprint. Discussion started: 21 March 2025

usable pictures, i.e. those not affected by excessive shadowing or unclean panel surface. To our knowledge, a time series of snow surface roughness properties was never measured before.

2.1.6 Snow Water Equivalent

Profiles of snow water equivalent (SWE) were sampled from the surface to the bottom with a cylinder cutter of inner diameter 9.44 cm and length 55 cm. The snowpack was sampled in sections from the surface to the ground and the total SWE was obtained by weighting each sample and summing up all the values. The uncertainty range of this instrument is around 10% with the main uncertainty source being caused by the presence of ice layers (Proksch et al., 2016).

2.2 Automatic measurements

2.2.1 Runoff

Runoff was automatically measured at a sub-hourly resolution by a lysimeter. Unfortunately, the instrument was discovered to be clogged when the runoff started in 2023. The instrument was repaired only in late May 2023. Therefore, the time series for that year starts with a peak (see Fig. 5d), although we hypothesize that runoff may have started as early as the end of April 2023. To avoid similar issues, on the following season the lysimeter was inspected timely and assessed as fully functional.

2.2.2 Snow Water Equivalent

Manual snow water equivalent (SWE) measurements are complemented by an automatically recorded time series at sub-hourly intervals, using the SSG1000 snow scale permanently installed at the WFJ site and manufactured by Sommer Messtechnik, Austria. The system consists of a weighing platform and load cells, which directly measure the weight of the snowpack on the platform and convert it into SWE. This instrument has a measurement range of 0 to 1000 mm of water equivalent. During the 2023-2024 snow season, the upper capacity was reached due to above-average snow depths. In comparison to manual measurements, Smith et al. (2017) estimated an error of $\pm 10\%$.

2.3 Sentinel-1 acquisitions

S1 is designed as a two sun-synchronous polar-orbiting satellite constellation, acquiring dual polarimetric C-band (frequency of 5.405 GHz, wavelength of 5.5 cm) SAR images with a nominal resolution up to 3.5 m × 22 m in Interferometric Wide swath mode (IW) and a revisit time of 6 days. Acquisitions in IW have a swat of approximately 250 km. This, together with the overlapping orbit paths, conceives the acquisition of multiple tracks at middle latitudes such as the Alps. For this reason, within the time window of 6 days, more acquisitions of the same area may be available. Four tracks are available for the area of Weissfluhjoch, and their main characteristics are summarized in Tab. 1.

The SAR images can be downloaded, free of charge, from the copernicus data hub (Copernicus). To account for the complex topography and to reduce the speckle noise of SAR acquisitions, a tailored preprocessing procedure has been applied to all data. The procedure uses a combination of tools, some are available in SNAP (Sentinel Application Platform) version 6.0 and

https://doi.org/10.5194/egusphere-2025-974
Preprint. Discussion started: 21 March 2025

Table 1. List of Sentinel-1 tracks over the WFJ field site, with times of acquisition and incidence angles.

Track number	Time of acquisition	Local incidence angle
015	Afternoon, ∼17:30	43°
066	Morning, ∼05:30	31°
117	Afternoon, ∼17:30	33°
168	Morning, ∼05:30	41°

some others are customized and written in Python. The procedure is listed and described in Marin et al. (2020). The final spatial resolution of the post-processed S1 images is 20 × 20 m.

2.4 Campaign design

Measurements were carried out within the same snow pit, which was always dug anew starting at approximately 08:00. The start of the measurement procedure depended on the amount of employees available on a specific day, on the amount of snow, on its density and on the weather conditions – generally, between one to two hours later. The measurement procedure was generally finished around 12:00 refilling the snowpit; however, on isolated days, there were several hours of delay because of the above mentioned reasons. On the first snow season, the snow temperature was generally measured first and the melting calorimetry last, with the remaining measurements being carried out in between with an order that also varied as a function of the above mentioned factors. On the second snow season, we improved the campaign design with a more rigorous measurement order: temperature first, SSA and dielectric LWC either simultaneously or one after the other, density, SWE, and melting calorimetry coupled with a second simultaneous dielectric LWC profile taken at the same time and vertical location. This has specific importance for the LWC profiles. On the first season, the time lag between the dielectric and calorimetric LWC profiles was 2 or 3 hours, at an horizontal distance of 50 cm to 1 m. On the second season, we measured one first dielectric LWC profile and an adjacent, simultaneous one using melting calorimetry. In Sec. 4.2, we will refer to the first setup as "co-located" and to the second one as "simultaneous".

On both seasons, before starting the measurement procedure, the profile wall was made as smooth as possible. A Near-Infra-Red picture was taken for qualitative comparison. Outside of the snow pit, on an undisturbed area, the surface roughness pictures were taken. On days where the radiation (from the sun or diffuse) was particularly intense, shading was necessary for every surface measurement that might have been affected. The temperature profiles were always measured in the shaded corner area of the snow pit. Overall, each measurement series would need a total horizontal space of 1.5-1.8 m, and the single variable profiles were measured at a reasonable horizontal distance from each other. On both seasons, snow profiles were carried out within the same designated area. The area was divided in corridors approximately 2 m wide. Throughout the season, measurements were carried out moving continuously forward along the corridor until the slope was hit. The next snow profile would be dug onto the next corridor. A minimum distance of 30 cm was secured between two consecutive measurement days, to avoid disturbances from the previous measurement set.

https://doi.org/10.5194/egusphere-2025-974
Preprint. Discussion started: 21 March 2025

Data cleaning and homogenization procedures were performed before providing the measured snow properties as RT inputs. In particular, since sampling resolutions were different (see Sec. 2.1), all measured properties were linearly interpolated to a common vertical resolution of 1 cm. Positive LWC values recorded at temperatures below 0°C were corrected to 0%. 0.04% and 0.4% of the measured LWC values were above or equal to 15% for the two years respectively. For both used dielectric instruments, these values are likely not accurate. Since these values likely represent areas of high snow wetness, they were not excluded from the analysis but their LWC value was set to 15%, similarly to Techel and Pielmeier (2011). Additionally, instances of very low LWC measurements from thin layers just above the ground in dry snow conditions were discarded, as we could not rule out potential instrument disturbances from the ground in these cases. Given the accuracy range of the thermometer (see Sec. 2.1), temperature oscillations up to 0.2°C below 0°C were set to 0°C from the first measured fully isothermal profile onwards. Since the snow properties were measured at a certain lateral distance one from the other, the profiles of density and SSA were slightly shifted with a simple algorithm to maximise the correlation with the profile of LWC. Finally, we had to discard the last 3 snowpits of 2023, because the measured RMSH value there was too high to ensure the conditions of validity of the interface model (see Sec. 3.2).

3 Methods and model

3.1 Selection of the Sentinel-1 reference cell

The selection of the reference S1 cell required some considerations. The WFJ field site is ideal for continuous measurements due to its proximity to structures and sensors, however, these features may interfere with radar waves thus disrupting the backscattering from natural terrain. Most of the structures within the field site are metallic and may act as additional reflecting sources in addition to the snowpack.

To select the reference cell, we extracted σ_0^{VV} values for both years over a grid of 56 points covering the whole extension of the field site and the immediate surroundings (Fig. 2a). For each cell and for each different year, we isolated the time frame starting at the beginning of the meteorological winter (December 01) and ending when the first liquid water was detected in the snowpack. Over these time frames, for each year and for each cell we computed the variability of σ_0^{VV} acquired by the 4 different tracks (See Tab. 1). We assume that low variability between different tracks over a dry snowpack may indicate a minimal interference with other non-natural elements on the field, as their backscatter would typically exhibit strong angular dependence (i.e. anisotropy).

The results of this analysis are summarized in Fig. 2. The variability is mapped over the field using the interquartile range (IQR). Each cell is represented by its centroid. The boxplots in Fig. 2 refer to the fraction having the 15% lowest average IQR and illustrate the variability of σ_0^{VV} for each single track and over the two snow seasons independently. In general, the IQR does not vary significantly between the two snow seasons, suggesting that this kind of approach might be adequate to select a reference cell with the least possible artificial disturbance. There are outliers (i.e. points 27, 52, 55) – however, such points are located in field areas likely affected by double-bounces effects typical of man-made targets (27) or surfacing boulders (52, 55), explaining the year-to-year variability. The highest IQR values are clustered around the large hut and where the slopes start

https://doi.org/10.5194/egusphere-2025-974
Preprint. Discussion started: 21 March 2025

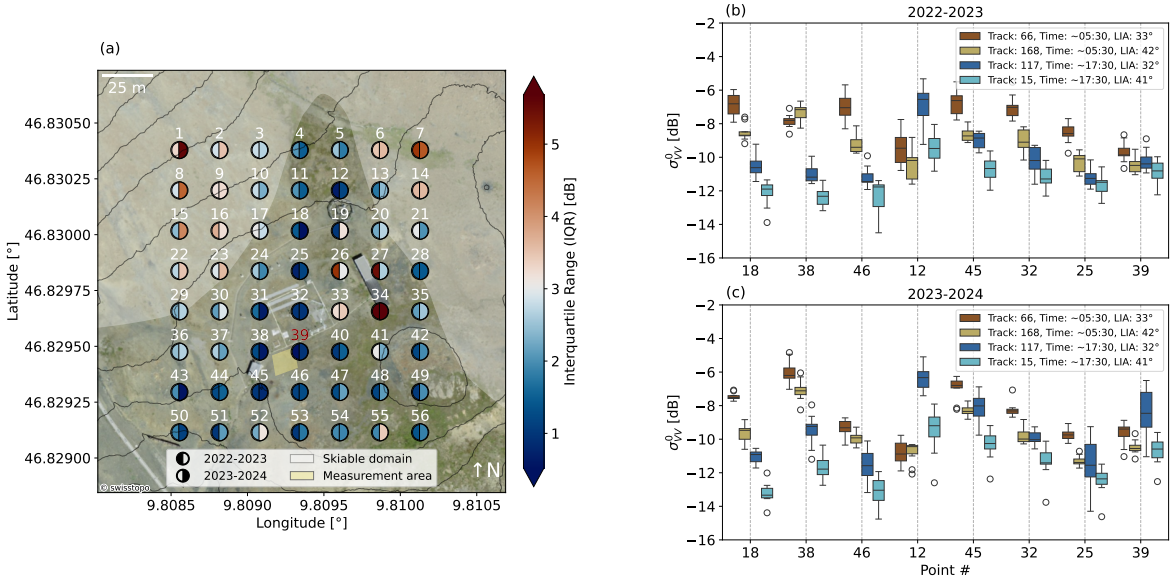

Figure 2. The map in a) shows an aerial view of the WFJ measurement station. Each of the 56 points represents the centroid of each S1 cell. Each centroid is split in two, the left part indicating the interquartile range (IQR) of the winter σ_0^{VV} signal for the snow season of 2022-2023 and the right part for the snow season of 2023-2024. Contour lines indicate the surrounding slopes. The area in white indicates the surrounding skiable domain. The yellow rectangle indicates the fenced measurement area where snow profiles were carried out in both seasons. Cell 39, i.e. the selected S1 cell for this study, is highlighted in red. The boxplots in b) and c) represent the variability of σ_0^{VV} (in dry conditions) over different tracks for the fraction of the S1 cells having the 15% lowest IQR, for the snow seasons of 2022-2023 and 2023-2024, respectively.

to become steeper, i.e. where the backscattering has a strong dependence on the aspect angle. Interestingly, the IQR values for cell 25 and 32 are among the lowest for both snow seasons, suggesting that smaller metallic sensors might not represent a disturbance for the radar waves. The boxplots in Fig. 2 show the variability of each single track for both years, ordered from higher to lower. Cells 38 and 45, despite having low IQR score for both snow seasons, show high σ_0^{VV} variability among different tracks, suggesting that the small hut, being relatively small with respect to the resolution cell, likely has a limited impact with respect to the bigger hut, but still generates a bias. Ideally, the target cell has a rather constant average σ_0^{VV} among all tracks and a low variability of each single track. These conditions are met by points 32, 25 and 39. Points 25 and 32 were discarded because they lie on a section of the field where the snow surface is regularly disturbed for daily measurements until complete snow ablation. Point 39, despite slightly overlapping with our measurement area, lies in close proximity of the measuring field, on a flat surface, protected from off-piste skiing and exhibits the lowest average IQR, the lowest spread in the average σ_0^{VV} value among all tracks, and the smallest overall variability of each single track, with a small exception for track

https://doi.org/10.5194/egusphere-2025-974
Preprint. Discussion started: 21 March 2025

117 over the season 2023-2024. For these reasons, the σ_0^{VV} recorded over cell 39 is selected as the reference time series for this work.

3.2 Snow Microwave Radiative Transfer (SMRT) model and simulation setup

SMRT is a model that simulates the active-passive microwave response from snowpacks (see Picard et al. (2018)). The model is written and run in a Python environment and has a modular and flexible structure, allowing the user to set model runs choosing among different electromagnetic, microstructure and permittivity models. The reflectivity and transmissivity associated to roughness can also be described according to different models. The user has to specify a set of snowpack properties to parametrize the microstructure and the electromagnetic model. In particular, the roughness can be set either at the snow-air interface only or for each defined snow layer. Once these necessary parametrizations have been declared in the preliminary components of the model, SMRT uses the discrete ordinate and eigenvalue (DORT) method to solve the radiative transfer equation. The user can either customize a virtual sensor with specific frequency, incidence angle and polarization or directly choose from a list of already available sensors, among which Sentinel-1. The backscattering intensities can be obtained for all polarizations – this study focuses on the co-polarized VV (vertical-vertical) signal, because cross-polarizations are currently only partially implemented within the current version of the module used for the parametrization of surface and interface scattering (Murfitt et al., 2024).

This study uses the symmetrized strong-contrast expansion (SymSCE) (Picard et al., 2022b) as the electromagnetic model with two different permittivity parametrizations. Measurements of density and SSA were used to compute the Porod length (ℓ_P) (Porod, 1951). The microwave grain size (ℓ_{MW}) is computed as the product of ℓ_P and the polydispersity k, a parameter describing the variability of the length scales with respect to the microstructure (Picard et al., 2022c). k was set to 0.75: this empirical value was estimated from μ-CT scans of a wide variety of Alpine snow samples with convex grains, among which rounded grains and melt forms (Picard et al., 2022c). As shown in Picard et al. (2022c), the choice of parametrization of the snow microstructure represents a secondary problem with respect to the ℓ_{MW} in order to predict snow scattering at C-band. For this study, snow microstructure was parametrized using the exponential model.

The permittivity of a material is a complex number composed of a real part (i.e. the dielectric constant) and an imaginary part. The contribution of the real part is related to the material's ability to store electrical energy, whereas the contribution of the imaginary part is associated with dielectric losses. Snow is a three-component mixture of snow, air and water – therefore, the effective permittivity of snow (ϵ_s) depends on the relative proportions of these elements. The presence of liquid water significantly alters both the real and imaginary parts of ϵ_s, affecting how microwaves interact with the snowpack. Henceforth, accurate estimates of ϵ_s are crucial for interpreting the microwave response of wet snow. Despite extensive research, particularly in the 1980s, a universally accepted model for snow permittivity remains elusive (Picard et al., 2022a). For this study, we selected two formulations: (i) the Microwave Emission Model for Layered Snowpacks version 3 (MEMLSv3 hereafter), which is based on the Maxwell-Garnett mixing theory of dry snow and prolate water inclusions; (ii) the Debye-like model modified by Hallikainen et al. (1986) by fitting it against field data (H-86 hereafter). These models were selected because they have been validated against real-world C-band data. Specifically, in Hallikainen et al. (1986) and earlier works, the authors present what

https://doi.org/10.5194/egusphere-2025-974
Preprint. Discussion started: 21 March 2025

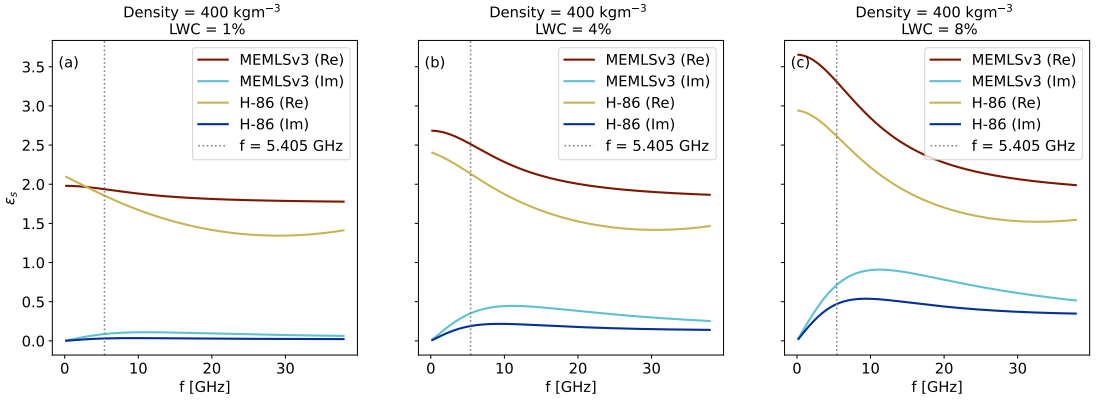

Figure 3. Real and imaginary parts of the effective permittivity (ϵ_s) of wet snow as a function of frequency (f) for a nominal density value of 400 kgm^{-3} and varying LWC of 1% (a), 4% (b) and 8% (c) according to the MEMLSv3 and H-86 permittivity models. Grey dotted lines underline differences between the formulations for the nominal frequency of S1, i.e. 5.405 GHz.

is, to our knowledge, the only available dataset of wet snow permittivity measurements at 6 GHz for varying LWC values, measured using freezing calorimetry. Interestingly, the MEMLSv3 fails to accurately reproduce this dataset. However, Kendra et al. (1998) observed that the dielectric constant provided by H-86 appears to be too low, an observation that is supported by data from Achammer and Denoth (1994), collected between 8 and 12 GHz. However, these data appear to favor H-86 over MEMLSv3 when considering the imaginary part of ϵ_s. While H-86 has been criticized, some aspects appear to have been overlooked (e.g. the recent corrigendum in Picard et al. (2022a)). Figure 3 shows the real and imaginary parts of the ϵ_s as a function of the frequency for a nominal density value and varying values of LWC according to both MEMLSv3 and H-86 permittivity formulations. For higher values of LWC (see Fig. 3b,c), the ϵ_s values obtained from both formulations display a frequency dependence and curve shape closely resembling that of pure water. In both cases, the real part of ϵ_s decreases with frequency, whereas the imaginary part increases up to the relaxation frequency and then decreases. However, at C-band, the two formulations diverge significantly, especially in their prediction of the imaginary part, which governs absorption losses. This difference becomes more pronounced for increasing values of LWC. For instance, at LWC =4%, MEMLSv3 predicts an imaginary part of ϵ_s approximately twice that of the H-86 at the nominal frequency of S1 (see Fig. 3b). Since we cannot definitively determine the fitness of one model over the other, both formulations will be used in the SMRT modeling for this study. Given the different behavior of the two formulations, we expect a lower and upper bound for S1 backscattering simulations. It is clear that further research is needed to accurately characterize wet snow permittivity, but this is out of the scope of this paper.

The chosen interface model (between snow and air and between snow layers) is the integral equation model (IEM) (Brogioni et al., 2010), since it is one of the most used models to describe the roughness. However, any other model could be used, provided the roughness characteristics are within the validity range. The IEM is valid under the conditions $w \cdot RMSH < 2$ and $w^2 \cdot RMSH \cdot CL < \sqrt{\varepsilon_i}$, where w is the wavenumber (which depends on the medium) and ε_i is the ratio between the media

https://doi.org/10.5194/egusphere-2025-974
Preprint. Discussion started: 21 March 2025

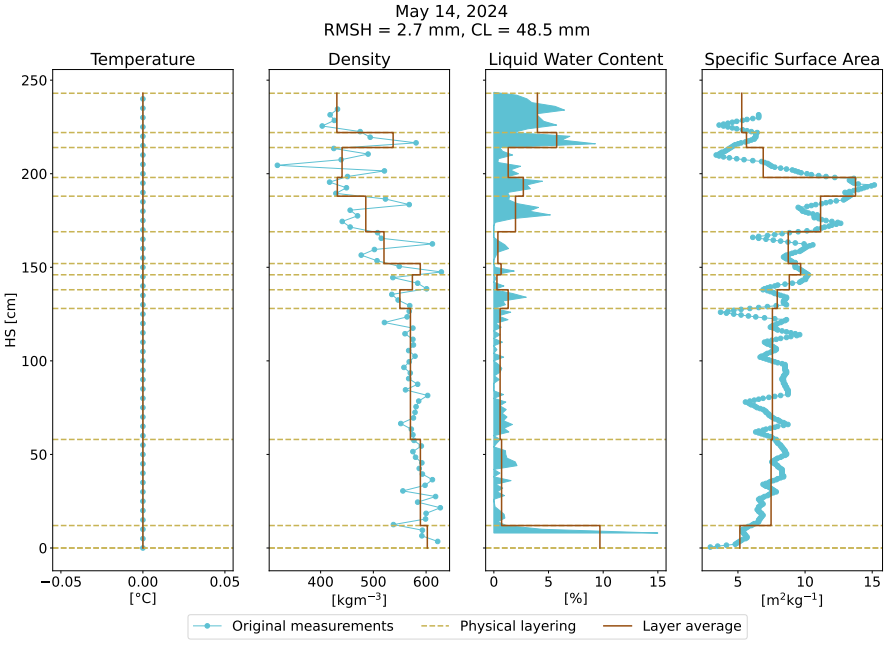

Figure 4. Example of a complete set of SMRT input snow properties for 14/05/2024: measured (light blue) and discretized with average values (brown) over identified physical layers (yellow).

permittivities at the interface (Fung et al., 1992). In the absence of rigorous information about the soil substrate, we modeled it as a frozen surface. We parametrized the soil backscattering for each year and incidence angle with an average of the values recorded by S1 from the start of the meteorological winter until the formation of liquid water within the snowpack, assuming that in dry snow conditions, the snowpack is almost totally transparent to C-band radar waves, and that therefore the soil is the only scattering source.

Under these configurations, the model takes as inputs the following snowpack properties: temperature, density, volumetric liquid water, SSA and roughness. For the snow-air interface, we used the measured values of RMSH and correlation length. For layer interfaces, we set $RMSH_{layers}$=1 mm and CL_{layers}=30 mm (i.e. the average winter value from our field measurements). When measurements and S1 overpasses coincided, the simulation was performed using the incidence angle of S1. On days without simultaneous overpasses, the simulation was performed using the incidence angle from the closest previous or subsequent S1 pass. All modeling choices described above have been designed and motivated to be optimal to describe wet snow starting from measured properties. However, it is important to remark that the choice of such parametrizations remains highly arbitrary, as further research is still needed to validate permittivity, roughness and microstructure models specifically for wet snow at C-band.

Another practical challenge was how to replicate the often complex snowpack layering observed in the field within a radiative transfer model which is not specifically made to deal with a high number of layers thinner than the wavelength (Sandells et al.,

https://doi.org/10.5194/egusphere-2025-974
Preprint. Discussion started: 21 March 2025

2022). As a matter of fact, this increases the number of dielectrical discontinuities (Leduc-Leballeur et al., 2015) generating (artificially) higher scattering. Resampling high resolution field measurements to the wavelength or its multiples is an option, however, this does not necessarily reflect the physical snowpack structure. As an example, in the moistening phase, liquid water appears in thin layers at the top of the snowpack. These layers can have thicknesses of a smaller size than the C-band wavelength: their scattering effect is unclear and this is a potential source of errors when using layering defined by the resolution of the field measurements. As the wetting front progresses through the snowpack during the ripening phase, liquid water becomes more homogeneous over thicker layers. During this phase, it might seem appropriate to choose high-resolution discretizations (e.g., comparable to the C-band wavelength) to reproduce as precisely as possible the liquid water layering observed in the field. However, this may artificially produce drier or wetter layers, potentially leading to a over or underestimation in backscattering, respectively. On the other hand, intuitively, lower-resolution discretizations (e.g., multiples of the C-band wavelength) dissipate the scattering effect of thinner ($\simeq$6 cm) wet layers. To reduce the aforementioned sources of uncertainty, we chose to model the snowpack structure by stacking layers with a minimum thickness corresponding to the C-band wavelength, ensuring each layer had consistent average physical properties. These property-based layers were identified automatically by means of a simple algorithm and then refined manually, with particular emphasis placed on LWC over the other variables. An example is given in Fig. 4. However, the optimal way to model a radar-equivalent snowpack from field measurements and/or detailed multilayer physical model outputs remains an open question in the field of radiative transfer modeling of snow, only recently addressed by Meloche et al. (2024), albeit for dry snow only.

4 Results

4.1 Snowmelt phases identification from multitemporal Sentinel-1 backscattering and field measurements

Fig. 5 and 6 show the evolution of the multitemporal S1 SAR backscattering together with the time series of measured properties: snow temperature, LWC, air temperature, total water content (TWC), runoff, snow water equivalent (SWE) and surface roughness indices (RMSH and CL). The melting phases identified with the method proposed by Marin et al. (2020) are reported on each time series for later validation. We will refer to the snow seasons of 2022-2023 and 2023-2024 as the 2023 and 2024 seasons, respectively.

Our measurement campaign brought us to observe that the roughness RMSH shows clear differences for different snow surfaces (Fig. 7). Smooth surfaces typical of new/dry snow have RMSH values around 1 mm (Fig. 7a). Thereon, the RMSH increases with increasing surface degradation due to melt-refreeze cycles and sublimation (Fig. 7b). The values of RMSH measured in these conditions, which are the most persistent throughout the melt season, lie within 3 and 10 mm approximately. Fully-formed suncups are associated to values of RMSH around 10-15 mm (Fig. 7c). Deep suncups appear like craters on the snow surface (Fig. 7d), some reaching width of 20 cm and depths of 10 cm. In these conditions, we measured values of roughness RMSH equal or higher than 20 mm.

In 2023, the first liquid water was measured on 10/04 (Fig. 5b,d). On this date, our data show that the temperature of the top $\sim$5 cm of the snowpack was 0°C (Fig. 5a). The air temperature reached 0°C as well on this day (Fig. 5c). The snowpack

https://doi.org/10.5194/egusphere-2025-974
Preprint. Discussion started: 21 March 2025

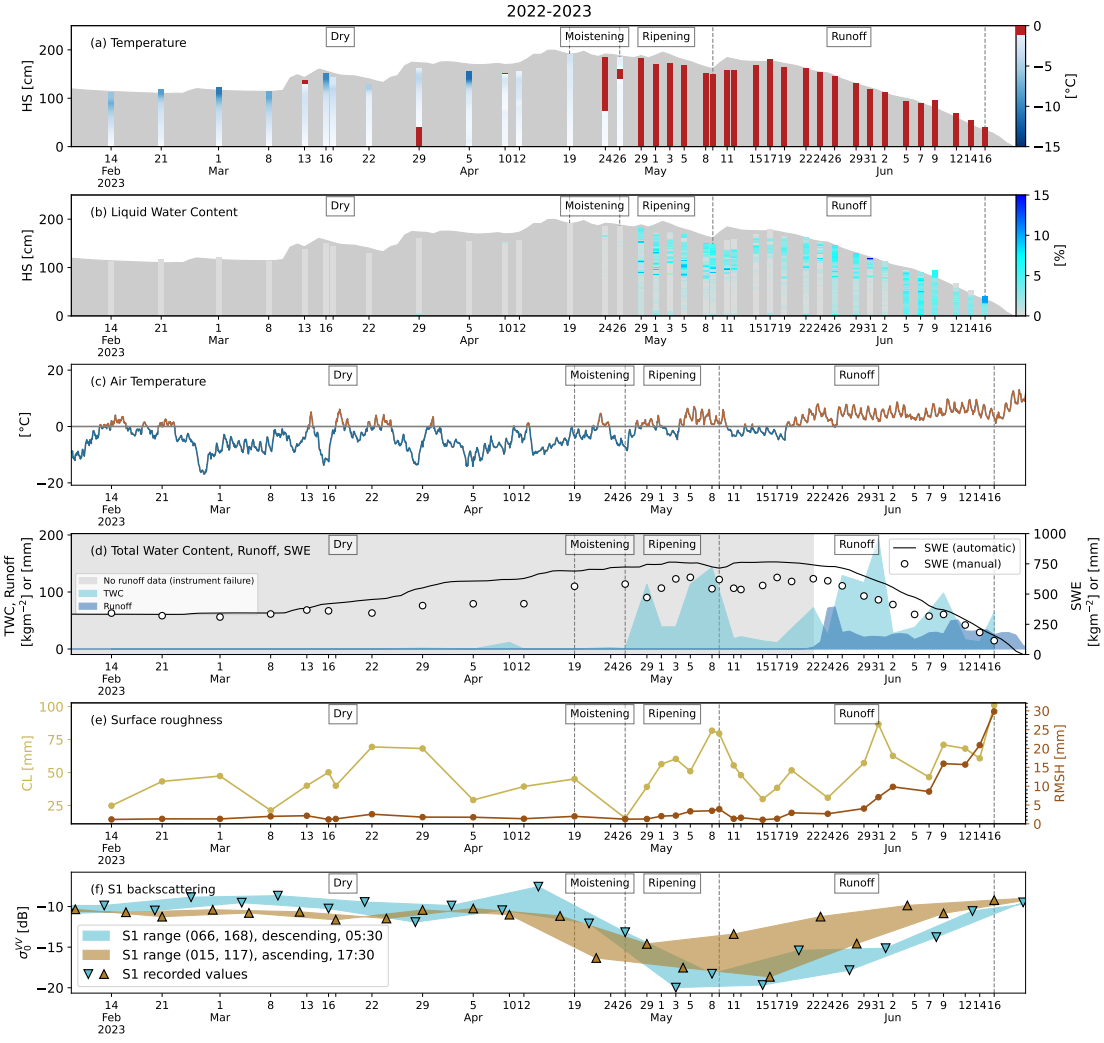

Figure 5. Data overview for the snow season of 2022-2023. Panel (a) shows the manually measured temperature profiles. Panel (b) shows the manually measured liquid water content (LWC) profiles. Panel (c) shows the air temperature at hourly resolution as measured by the automatic sensor at WFJ. Panel (d) shows the measured total water content (TWC) (light blue), the runoff time series automatically recorded by the lysimeter (dark blue), the snow water equivalent (SWE) both automatically recorded (black line) and manually measured (black points), and the lack of runoff data due to the instrument failure (grey area). Panel (e) shows the measured time series of surface roughness by means of the two indices RMSH and CL. Panel (f) shows the recorded S1 time series divided into descending morning (light blue) and ascending afternoon (light brown) passages. In panel (f), the triangles indicate the exact values of S1 acquisitions, whereas shaded areas represent the range of σ_0^{VV} values obtained by connecting the consecutive S1 passages by direction of orbits, i.e. by connecting all the morning/descending and the afternoon/ascending acquisitions. Each panel is subdivided into the melting phases identified according to the method of Marin et al. (2020).

https://doi.org/10.5194/egusphere-2025-974
Preprint. Discussion started: 21 March 2025

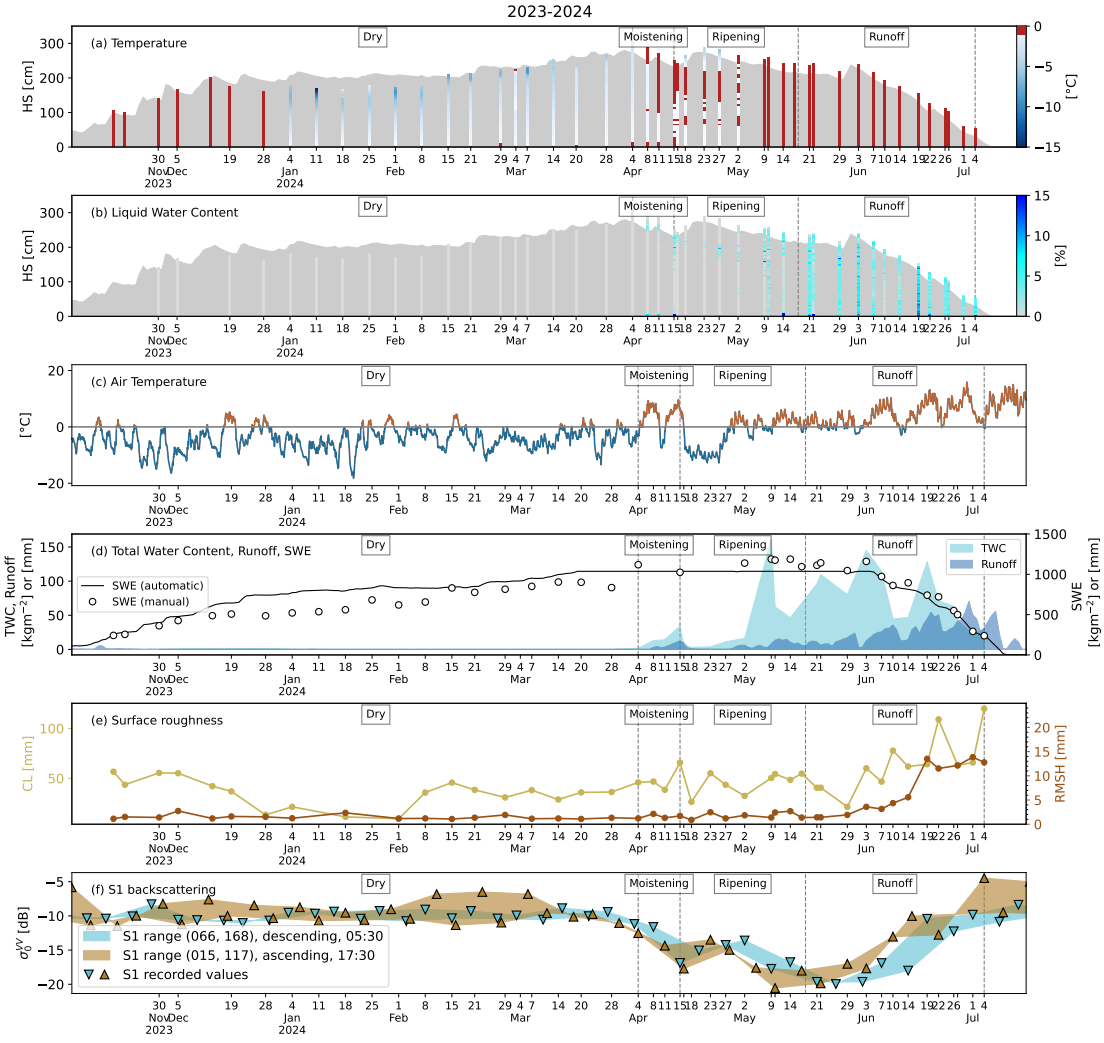

Figure 6. Data overview for the snow season of 2023-2024. Panel (a) shows the manually measured temperature profiles. Panel (b) shows the manually measured LWC profiles. Panel (c) shows the air temperature at hourly resolution as measured by the automatic sensor at WFJ. Panel (d) shows the measured total water content (TWC) (light blue), the runoff time series automatically recorded by the lysimeter (dark blue), the snow water equivalent (SWE) both automatically recorded (black line) and manually measured (black points). Panel (e) shows the measured time series of surface roughness by means of the two indices RMSH and CL. Panel (f) shows the recorded S1 time series divided into descending morning (light blue) and ascending afternoon (light brown) passages. In panel (f), the triangles indicate the exact values of S1 acquisitions, whereas shaded areas represent the range of σ_0^{VV} values obtained by connecting the consecutive S1 passages by direction of orbits, i.e. by connecting all the morning/descending and the afternoon/ascending acquisitions. Each panel is subdivided into the melting phases identified according to the method of Marin et al. (2020).

https://doi.org/10.5194/egusphere-2025-974
Preprint. Discussion started: 21 March 2025

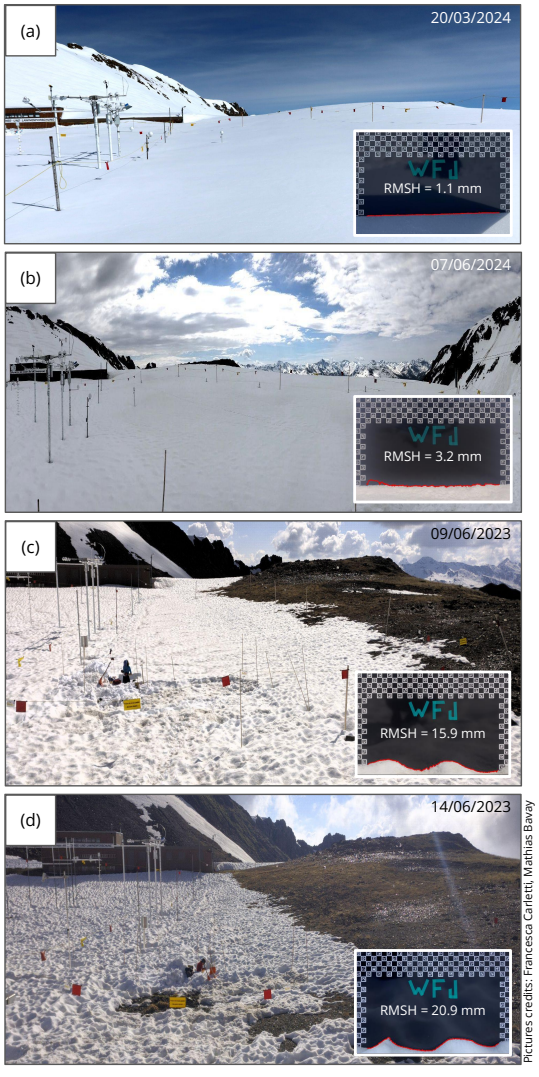

Figure 7. The panels illustrate some representative surface roughness conditions as qualitatively observed on the field (panoramic pictures) together with one of the panel measurements performed on the same day (bottom right of each panel, where the mean roughness RMSH measured on that day is also reported). Panel (a) shows a smooth surface typical of dry snowpack conditions. Panel (b) shows early-stage development of surface roughness deriving from melt-refreeze cycles. Panel (c) shows fully-formed suncups over a homogeneous snow cover, at least among the considered S1 cell. Panel (d) shows fully-formed suncups over a mostly patchy snow cover.

reached full isothermal state 20 days later. Ice layers formed throughout the season, likely as a consequence of repeated melt-refreeze cycles and the succession of several warm and cold spells (Fig. 5c). Ice layers were observed regularly during the measurement campaign, their presence is highlighted by locally higher values of LWC due to ponding at approximately 100 cm from the ground. The presence of ice layers probably withheld the meltwater in the upper section of the snowpack, partially

https://doi.org/10.5194/egusphere-2025-974
Preprint. Discussion started: 21 March 2025

hindering the progression of the wetting front. LWC profiles in Fig. 5b highlight ponding above ice layers consistently until 15/05. The ponding is no longer detected over the next consecutive 5 snow profiles and becomes visible again from 26/05 until early June, when the ice layers likely disintegrated allowing the meltwater to percolate to the bottom of the snowpack. The fact that the ponding above ice layers is not detected on a series of consecutive snow profiles is probably linked to the partial refreeze of the snowpack highlighted by the drop in air temperature detected within this time span (Fig. 5c). However, ice layers could also be laterally non homogeneous. Fig. 5 shows that the roughness associated with wet snow starts developing short after the snowpack starts moistening, with RMSH increasing until 09/05. Then, starting from 09/05, the cold spell brought new snowfalls which smoothened the snow surface significantly, and roughness indices reverted to typically winter values for approximately 10 days. Fully-formed suncups were observed on the field from 31/05 onwards. As explained in Sec. 2.2, the lysimeter time series for 2023 (Fig. 5d) is not useful to detect the runoff start. However, the automatic measurements indicate the first slight SWE decrease around 08/05, following a warm spell that lasted several days. This occurred in the presence of a fully isothermal snowpack, suggesting that meltwater may have started to be released around this time.

In 2024, the first liquid water on the surface was measured on 08/04 during a warm spell (Fig. 6b,c,d). From this date on, the wetting front moved somewhat into the snow before being interrupted by a cold spell, which caused a partial surface refreeze (Fig. 6a,b,c). The snowpack reached the full isothermal state on 09/05. Over the course of this season, ice layers were not observed in the field, the progression of the wetting front was not hindered and the snowpack reached full saturation earlier with respect to the previous year. The runoff time series confirms that the snowpack released the first meltwater around 08/04 – on this date, the (point-wise) measurements show a largely isothermal snowpack. Likely, the snowpack was isothermal over the entire cell (see Fig. 6a,b,d). Additionally, significant amounts of LWC were measured at the ground interface after 08/04 and the manual measurements show a SWE decrease of $\simeq$100 mm between 04 and 15/04. These observations can validate the same hypothesis made for the previous season in the absence of runoff data due to instrument failure. Fig. 6e shows that we measured increasing surface roughness relatively late (03/06) with respect to the previous season, with fully-formed suncups being visible on the field from 19/06 onwards.

Coupling the detailed, high temporal resolution information about the state of the snowpack with the multitemporal SAR σ_0^{VV} recorded by S1 on morning and afternoon overpasses (Fig. 5-6f) enables the validation of the methodology proposed by Marin et al. (2020) to identify the melting phases. According to the authors, a drop of at least 2 dB with respect to the winter mean in the afternoon σ_0^{VV} identifies the start of the moistening phase; the ripening phase starts when the morning σ_0^{VV} signal shows the same drop of at least 2 dB; the runoff starts when both morning and afternoon σ_0^{VV} time series reach their local minima before the monotonic increase (the authors propose an average date between the two local minima when both the S1 satellites were available). To obtain the average winter backscattering ($\overline{\sigma_{0,dry}^{VV}}$) for the two seasons, we considered all values recorded by all tracks over the meteorological winter, i.e. from 01/12 until 28/02. This is the threshold needed to identify the melting phases, which are summarized in Table 2. As noted by Marin et al. (2020), the dependence of σ_0^{VV} on incident and aspect angles remains as a residual effect. While the overall magnitude does not change significantly, it would be more precise, in theory, to compute four separate values for $\sigma_{0,dry}^{VV}$, one for each track. However, our selection of the reference cell was

https://doi.org/10.5194/egusphere-2025-974
Preprint. Discussion started: 21 March 2025

Table 2. Overview on the identification of the melting phases based on the multitemporal S1 SAR backscattering as proposed by Marin et al. (2020). For each season, the table shows the relevant values of σ_0^{VV} and the occurrence dates. For the runoff start, the date proposed by Marin et al. (2020) is compared against the data from the lysimeter, when available.

Season →	2022-2023		2023-2024	
Event ↓	[dB]	Date	[dB]	Date
$\overline{\sigma_{0,dry}^{VV}}$	-9.7	01/12 - 19/04	-10.4	01/12 - 04/04
Moistening start	-11.2 ∼ -17.5	19/04	-12.5	04/04
Ripening start	-13.2	26/04	-16.9	15/04
$\sigma_{0,min,afternoon}^{VV}$	-18.7	16/05	-20.6	10/05
$\sigma_{0,min,morning}^{VV}$	-19.9	03/05	-19.9	26/05
	Marin et al. (2020)	Lysimeter	Marin et al. (2020)	Lysimeter
Runoff start	09/05	No data – ∼29/04 (?)	18/05	∼15/04

guided by minimizing the influence of aspect and incidence angles on the winter σ_0^{VV} as discussed above (see Fig. 2b). As a result, we chose to use a single, averaged value of $\overline{\sigma_{0,dry}^{VV}}$ over the 4 tracks.

The method of Marin et al. (2020) is challenged by the low S1 revisit frequency provided by only one satellite. In detail, for the moistening start in 2023, σ_0^{VV} recorded on 17/04 is only 1.5 dB lower than $\overline{\sigma_{0,dry}^{VV}}$, whereas on the next passage the drop is 7.8 dB already. For this reason, the moistening start for 2023 has been placed on the date in between, namely 19/04. Moreover, due to the lower satellite revisit time, the separations between local minima are 13 and 16 days for 2023 and 2024, respectively. Using the date in between to determine the runoff start, as done by Marin et al. (2020), gives potentially unreliable results in these conditions. This low temporal resolution makes it difficult to pinpoint precise onset dates, especially when minima are separated by such long periods. Despite the ambiguities, on both seasons, the identified moistening phase coincides exactly with the first snowpack warming and the consequent formation of liquid water. The identified ripening phase is also mostly consistent with the theory, as field measurements show that the snowpack transitions to the fully isothermal state with the wetting front progressing to the bottom, although this process is partially hindered in 2023 by ice layers. In 2024, a sudden cold spell at the beginning of the ripening phase caused the refreezing of the superficial meltwater (Fig. 6a,b,c). This generated a sharp increase in both morning and afternoon σ_0^{VV} (Fig. 6f). In 2024, the first instance of measuring a fully isothermal snowpack coincided precisely with the first afternoon local minimum of σ_0^{VV}. The positive bias of the track 117 due to its low incidence angle does not allow to verify the same for 2023 and it creates a counterintuitive case where the local minimum of morning σ_0^{VV} anticipates the local minimum of afternoon σ_0^{VV} (Fig. 5f). Nonetheless, by the time the morning σ_0^{VV} reached its local minimum in 2023, the snowpack had already been fully isothermal for at least 5 days (Fig. 5a,f). This suggests that the snowpack is likely to be fully isothermal when the afternoon backscattering reaches its local minimum. The runoff time series in 2024 shows that the snowpack had started to release meltwater as soon as in the late moistening phase (Fig. 6d), in correspondence of the first local minimum of the multitemporal SAR backscattering on 16/04 (Fig. 6f).

https://doi.org/10.5194/egusphere-2025-974
Preprint. Discussion started: 21 March 2025

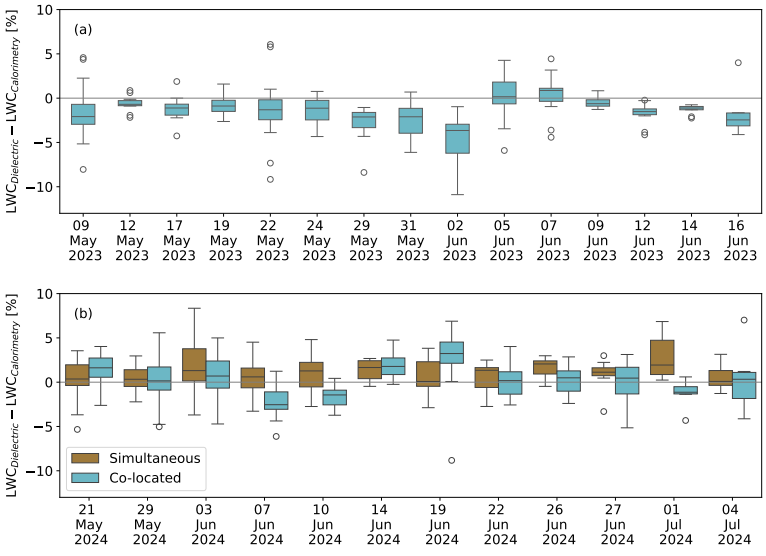

Figure 8. Bias between liquid water content measurements with dielectric devices and melting calorimetry for snow seasons of (a) 2023 and (b) 2024. In 2024, direct comparisons between simultaneous (brown) and co-located (light blue) measurements are available.

Marin et al. (2020) proposed three possible explanations for the monotonic backscattering increase following the local minima: (i) the increase in surface roughness, (ii) the decrease in TWC and (iii) the snow cover gradually becoming patchy. Our data show that over a high-altitude alpine snowpack like the study plot at WFJ, surface roughness develops well in advance of when the snow cover begins to disappear in patches. Therefore, at least for similar altitudes, the gradual disappearance of the snow cover can be ruled out as a cause of the increasing backscattering in the late melting stage. For both seasons, our data indicate that the strongest correlation with the monotonic increase of σ_0^{VV} after the local minimum is observed with the gradual increase in surface roughness (Fig. 5-6e). Conversely, there seems to be no remarkable correlations between the increase in σ_0^{VV} and the TWC and/or runoff trends. In fact, Fig. 5-6d show that the decrease of TWC as a consequence of snow ablation is not monotonous. On the other hand, both automatic and manual measurements show that by the time SWE started decreasing monotonically (around 26/05/2024 and 06/06/2024), the S1 σ_0^{VV} had already increased again by $\simeq$5 dB.

4.2 Instrumental uncertainty and variability in field measurements of liquid water content

Fig. 3 shows that liquid water has a strong impact on the real and imaginary parts of the effective permittivity of snow at C-band frequencies, and therefore, on radiative transfer modeling. For S1 σ_0^{VV} retrievals from ground measurements, this poses three major challenges. In the first place, manual measurements concern a very small area/volume whereas satellite acquisitions cover a pixel size of 20 × 20 m. Secondly, the distribution of liquid water within the snowpack can be highly heterogeneous because of a variety of features and processes, namely capillary barriers, preferential flows, ice layers. Finally, what is the

https://doi.org/10.5194/egusphere-2025-974
Preprint. Discussion started: 21 March 2025

Table 3. Bias (in dB) between modeled and S1 recorded σ_0^{VV} values according to the snow season, the selected permittivity formulation and melting phase.

Season →	2022-2023			2023-2024		
Permittivity formulation →	H-86	MEMLSv3	Data to compare	H-86	MEMLSv3	Data to compare
Bias ↓	[dB]	[dB]	[#]	[dB]	[dB]	[#]
Overall	5.37	6.57	12	6.83	7.86	26
Dry	1.00	1.35	5	0.56	0.57	4
Moistening	–	–	0	11.21	11.31	3
Ripening	5.17	6.96	4	9.37	12.00	8
Runoff	8.84	10.24	3	4.03	3.43	11

most accurate methodology for measuring LWC in both lab and field environments remains a debated question in snow science (Barella et al., 2024), and although the methods used in this paper attempt to achieve a good level of reliability, they are nevertheless subject to error. Therefore, all these uncertainty sources need to be taken into account when comparing satellite σ_0^{VV} retrievals with measured data.

In Sec. 2.4, we explained how dielectric measurements were validated against melting calorimetry in conditions of ripe snow. We referred to the validation setup of 2023 as "co-located" only; whereas in 2024 we performed an additional "simultaneous" validation in addition to the co-located. Figure 8 shows the spread between dielectric and calorimetric measurements in co-located and simultaneous setups for all the LWC validation measurements made over the two years. In 2023, the average maximum bias between co-located measurements is 2.6% and the average standard deviation is 1.2%. In 2024, the average maximum bias and the average standard deviation are 2.6% and 1.4% for co-located measurements and 2.3% and 1.5% for simultaneous measurements, respectively. Figure A1 shows all the measured vertical profiles in detail. In 2023, there is an overall good agreement between dielectric and calorimetric measurements. The time lag between the measurements is highlighted by often similar LWC profile shapes, with calorimetry generally measuring higher peak values. Unexpectedly, in 2024, the simultaneous measurements resulted in only slightly lower biases and slightly higher standard deviations. This result is supported by a number of previous studies. For example, Donahue et al. (2022) found an average standard deviation of 1% over 10 cm wide snow samples with LWC between 0 and 5%. The study of Techel and Pielmeier (2011) confirms the high occurrence of measurement deviations of more than 1% at short horizontal distances. However, Techel and Pielmeier (2011) also show that the correlation between measurements at larger horizontal distances is higher for LWC values lower than 1.3%. Therefore, the biases and standard deviations observed in our field measurements may overestimate the instrument uncertainty and/or variability over larger scales comparable to the footprint of S1. Based on these considerations, we define the large-scale LWC variability as $\pm 1\%$. We use this value to assess the effect of LWC uncertainty on σ_0^{VV} retrievals from ground measurements.

https://doi.org/10.5194/egusphere-2025-974
Preprint. Discussion started: 21 March 2025

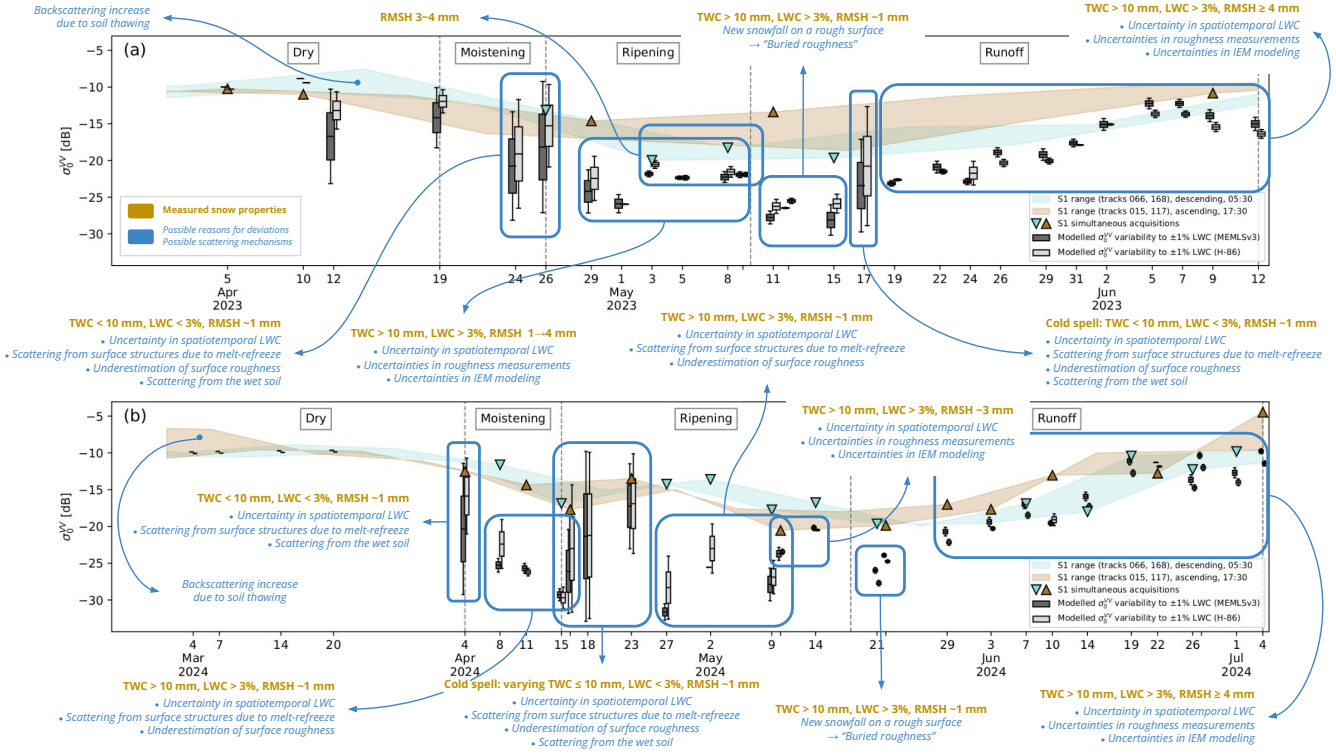

Figure 9. Recorded S1 multitemporal σ_0^{VV} (light blue and light brown triangles and shaded areas) compared against SMRT modelled values of σ_0^{VV} using MEMLSv3 (dark gray boxplots) and H-86 (light gray boxplots) permittivity models. The boxplots indicate the variability of the results considering an uncertainty of $\pm 1\%$ in the LWC values for each layer (see Sec. 4.2). The shaded areas of the recorded S1 multitemporal σ_0^{VV} represent the range of σ_0^{VV} values obtained by connecting the consecutive S1 passages by direction of orbits, i.e. by connecting all the morning/descending and the afternoon/ascending acquisitions. The triangles represent the exact values of the acquisitions. For clarity, exact values are only shown for days where snow profiles were carried out and therefore simulation and direct comparison is possible. Blue boxes group similar simulation results together. Yellow bold text indicates the measured snow properties for each result group, whereas blue italic text explains possible backscattering mechanisms which may have originated the (spread of) simulated results.

4.3 Interpretation of Sentinel-1 backscattering through SMRT simulations driven by field measurements

Figure 9 shows the comparison between the S1 acquisitions and the modeled σ_0^{VV} driven by snowpit measurements using the two different permittivity models MEMLSv3 and H-86 in SMRT and the model setup described in Sec. 3.2 considering the LWC variability of $\pm 1\%$ estimated in Sec. 4.2. In this Figure, we divided the simulation results into groups and discuss possible driving mechanisms and/or deviations from S1 for each group based on the measured values of LWC, TWC and surface roughness. We show all measured profiles of LWC with the relative measured values of TWC and RMSH values in Fig. 10 and Tab. 4, which will serve as a reference in the following explanations. Tab. 3 shows all biases between S1 acquisitions and simulations, according to the snow season, the selected permittivity formulation and the melting phase. In general, both models

https://doi.org/10.5194/egusphere-2025-974
Preprint. Discussion started: 21 March 2025

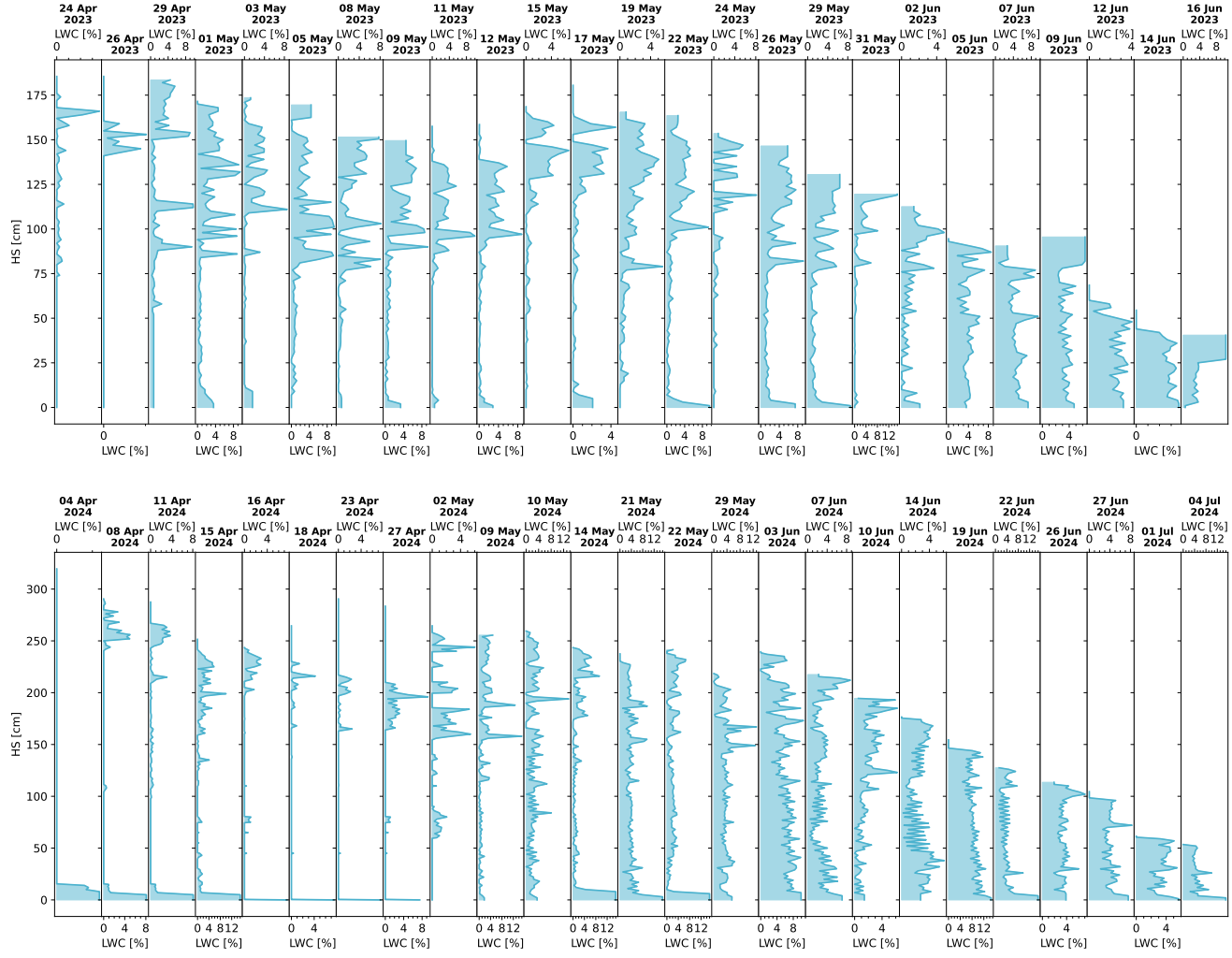

Figure 10. Ensemble of all the measured LWC profiles from 24/04/2023 and 04/04/2024, i.e. the first dates for which a significant discrepancies between modeled and S1-acquired σ_0^{VV} values are recorded in 2023 (top row) and 2024 (bottom row), respectively (see Fig. 9).

exhibit a mean negative bias of 6 dB with respect to S1 recordings over both seasons; however, biases are more pronounced for 2024 than for 2023, with the deviation between permittivity models being higher as well in 2024. H-86 generally gives higher σ_0^{VV} values with respect to MEMLSv3.

In 2023, the #066 morning S1 track recorded a backscattering increase of more than 2 dB between 05 and 19/04. Similarly, in 2024, we observe a 2.5 dB increase in backscattering recorded track #117 from 08/02 to 04/03. We can hypothesize that such increases are driven by the thawing of the soil. However, our data are insufficient and too uncertain to prove so, because of the possible interferences between dielectric instruments and the ground in mostly dry snow conditions, as mentioned in

https://doi.org/10.5194/egusphere-2025-974
Preprint. Discussion started: 21 March 2025

Table 4. Total Water Content (TWC) and Surface Roughness (RMSH) values measured on the same dates as the LWC profiles shown in Fig. 10.

Year →	2023																								
Month →	Apr			May														Jun							
Day →	24	26	29	01	03	05	08	09	11	12	15	17	19	22	24	26	29	31	02	05	07	09	12	14	16
Value ↓																									
TWC [mm]	3	1	113	39	39	114	143	102	18	22	14	11	36	72	24	129	116	193	27	38	67	98	16	13	64
RMSH [mm]	3	1	1	2	2	3	3	4	1	2	1	1	3	–	3	–	4	7	10	–	9	16	16	21	30

Year →	2024																								
Month →	Apr								May							Jun								Jul	
Day →	04	08	11	15	16	18	23	27	02	09	10	14	21	22	29	03	07	10	14	19	22	26	27	01	04
Value ↓																									
TWC [mm]	2	13	14	34	6	3	4	11	16	161	62	46	96	110	80	145	115	44	47	129	71	63	42	22	29
RMSH [mm]	1	2	1	2	–	1	2	1	2	1	2	3	1	1	2	4	3	4	6	14	12	–	12	14	13

Sec. 2.1.4. In dry snow conditions, there were no significant discrepancies between S1 and simulations during the dry seasons; henceforth Fig. 9 only focuses on the period after the assumed soil thawing.

Aside the chosen permittivity model, five primary sources of uncertainty may account for the differences between simulated and recorded σ_0^{VV}. In the first place, we should consider the fact that a significant source of uncertainty between recorded and modeled σ_0^{VV} values is snow transformation and melting between satellite and measurement acquisitions. S1 orbits intersect the field area either in the early morning or in the late afternoon (see Tab. 1). As explained in Sec. 2.4, measurements started at around 10:00 and would take several hours. Thus, it is likely that in both cases the LWC during the passage is lower than the value measured at 10:00 or later because of daily melt-refreeze cycles, especially near the snowpack surface. Moreover, the point-wise LWC measurements are not necessarily representative of the general liquid water distribution on the entire S1 pixel. In 2023 we consistently observed ice layers over a high number of consecutive snow profiles (see Fig. 5b and 10). Our consecutive measurements suggest that ice layers contributed to creating a more spatially homogeneous liquid water distribution by acting as a natural drainage barrier for meltwater. Unlike 2023, in 2024 ice layers were not consistently observed in the field. Likely, the melting process has been more heterogeneous over the cell area of 20 × 20 m, and point-wise measurements are less representative of wider scales on this season. This explains the fact that days marked by high variability associated with LWC are more numerous in 2024 than in 2023. In Fig. 9, we grouped these sources of uncertainties together under the labels "uncertainty in spatiotemporal LWC". Potentially, this source of uncertainty affects every S1 retrieval from field data. However, it definitely carries more weight than other sources of error at early melt stages when the simulation variability associated to LWC uncertainty is particularly high, i.e., when the TWC is low (24 to 26/04/2023, 04/04/2024) and during both the cold spells of 2023 (17/05) and 2024 (15 to 23/04), which caused the partial refreeze of the snowpack (see Fig. 5-6a,b,c).

Daily melt-refreeze cycles, however, not only alter the amount of LWC/TWC in the snowpack, but they also drive the formation of surface structures that can create additional scattering which is not accounted for in the simulations, i.e. crusts (Lund et al., 2022; Brangers et al., 2024). In Fig. 9, we labeled this uncertainty source as "scattering from surface structures

https://doi.org/10.5194/egusphere-2025-974
Preprint. Discussion started: 21 March 2025

due to melt-refreeze". This uncertainty applies to the same cases as where "uncertainty in spatiotemporal LWC" applies, but it likely holds more weight when the TWC is slightly higher and the simulation variability according to LWC is lower (08 to 15/04/2024, 27/04 to 09/05/2024).

Another cause of significant discrepancy between recorded and modeled σ_0^{VV} in the presence of a mostly dry snowpack with a smooth surface may be the thawing of the soil. This process creates a thin layer of liquid water overlying the natural soil roughness or absorbed into the basal snow layer (Lombardo et al., 2025). The combination of snow wetness and roughness, as will be shown later in the paper, can be responsible for backscattering increases up to 7 dB. In Fig. 9 we refer to this kind of uncertainty as "scattering from the wet soil". This uncertainty potentially applies to the instances when the TWC is relatively low and the variability associated to LWC is high. Between 04 and 27/04/2024, our measurements show considerable amounts of liquid water at the soil interface with otherwise relatively dry snowpack and smooth surfaces (see Fig. 10). The lysimeter time series corroborates these measurements by detecting runoff start on 08/04/2024 (see Fig. 6d). However, we lack sufficient data in order to prove and explore this possible scattering source, therefore we mention it only as an hypothesis.

Two similar instances in 2023 (05 to 09/05) and 2024 (10 and 14/05) suggest another interesting phenomenon likely affecting simulation accuracy. On both these intervals, Fig. 9 shows very good agreement between recorded and modeled values of σ_0^{VV}, regardless of the chosen permittivity model and the variability associated to LWC. On both instances, surface roughness had just started developing on a wet snow surface ($LWC > 3\%$), with measured RMSH values between 3 and 4 mm (see Fig. 7b). Thereafter, spring snowfalls cover the early-stage roughness and the snow surface reverts to smooth with RMSH values between 1 and 2 mm (see Fig. 7a). On both years, the group of simulations following the spring snowfalls (i.e. 11 to 15/05/2023 and 21 and 22/05/2024) show again strong biases when compared to S1 recordings. This bias is almost certainly due to the fact that the surface roughness which had started to develop is now buried below a smooth layer of new snow and it is not simulated by SMRT in the proposed configuration (see Sec 3.2). In Fig. 9 we labeled this phenomenon as "buried roughness".

Generally, simulations are in better agreement with S1 recordings when the measured surface RMSH is above 3 mm. Fig. 9 shows multiple groups of simulations where S1 retrievals from field data gain increasing accuracy with increasing RMSH on a wet surface, together with a decreasing dependence on the chosen permittivity model and the uncertainty associated to LWC (29/04 to 09/05/2023, 19/05 to 09/06/2023 and 29/05 to 01/07/2024). These instances suggest that in conditions of increasing surface roughness on a wet snow surface, additional source of uncertainty in S1 retrievals from field data might be associated to the IEM modeling (see Sec 3.2) translating surface roughness in backscattering response and/or to point-wise panel measurements underestimating the surface roughness of the entire S1 cell. In this sense, the fact that the chosen reference cell might slightly overlap with the snow surface disturbed by snow profile digging is another factor to consider to explain discrepancies between S1 recordings and retrievals. In Fig. 9 we labeled these sources as "uncertainties in IEM modeling" and "uncertainties in roughness measurements", respectively.

Interestingly, the S1 signal saturates on both years at values of σ_0^{VV} around $\sim$-20 dB, which is close to the nominal noise equivalent sigma naught (NESZ) of S1, i.e. -22 dB. The saturation of the signal is obtained by SMRT at much lower values, around $\sim$-30 dB, regardless of the chosen permittivity model.

https://doi.org/10.5194/egusphere-2025-974
Preprint. Discussion started: 21 March 2025

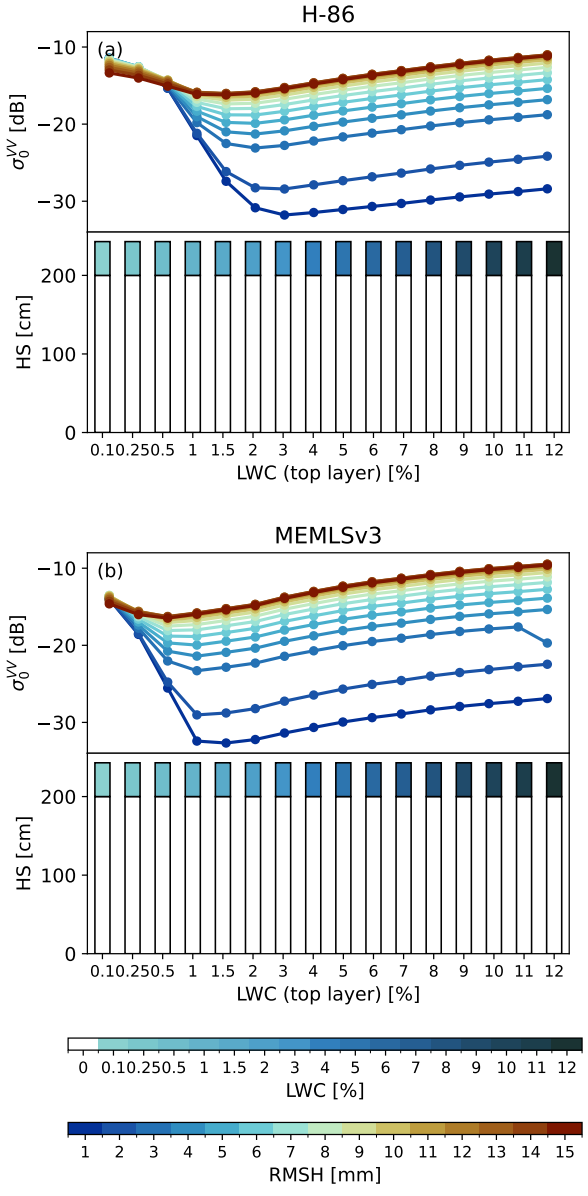

Figure 11. C-band radar backscattering sensitivity to the coupled evolution of surface roughness (expressed by RMSH) and LWC according to (a) H-86 and (b) MEMLSv3 formulations. The top part of each panel shows the sensitivity of σ_0^{VV} to consecutive synthetic snowpack variations. The real reference case is the snowpack layering observed on 16/04/2024: a melt event in the superficial 45 cm and an otherwise dry snowpack. The bottom part of each panel shows the consecutive snowpack synthetic variations in terms of surface LWC.

https://doi.org/10.5194/egusphere-2025-974
Preprint. Discussion started: 21 March 2025

4.3.1 C-band radar backscattering sensitivity to the coupled evolution of surface roughness and liquid water content

To study the C-band radar backscattering sensitivity to the coupled evolution of surface roughness and LWC, we selected the date of 16/04/2024. On this date, we measured a melt event in the superficial 45 cm. The bottom part of the snowpack was homogeneously dry and was discretized as a one layer with the average of the scattering properties measured in the field. These values are representative of a compacted snowpack structure at the beginning of the melt process: density of 428 kgm^{-3}, SSA of 15.1 m^2kg^{-1} and temperature of -0.1 °C. From this configuration, we prepared a series of synthetic snowpack variations with surface LWC increasing from 0 to 12%, and coupled each of them with a range of surface roughness RMSH increasing from 1 to 15 mm. The extremes of the explored surface roughness range represent a smooth surface characteristic of recent snowfall and the highly textured surface of fully formed suncups, respectively. To ensure consistency, we gradually increased the value of the second roughness parameter CL as well. To do so, we used an empirical logarithmic relationship extracted from field data between RMSH and CL, which we report in Fig. A2. However, this empirical relationship is based on a limited number of points (75 in total) which show larger spreads for increasing values of RMSH. Therefore, we assume that the only discontinuity in the experiment results (see Fig. 11b, $RMSH$ =3 mm and LWC_{top} =12%) can be explained considering this uncertainty. We run all experiments with the same incidence angle of 41°. The result of all the experiments is shown in Fig. 11 for both permittivity formulations.

In general, Fig. 11 shows that the intensity of the scattering response has a strong dependence on LWC for lower values of surface roughness ($RMSH \leq$3 mm). The higher the surface roughness, the weaker the dependence on LWC. More in detail, with H-86, for LWC values lower or equal to 0.5%, simultaneously increasing surface LWC and surface roughness causes a decrease in C-band σ_0^{VV} of a maximum of 2 dB. Within this range, the intensity of the σ_0^{VV} drop from smooth to rough surfaces decreases gradually with increasing LWC. For LWC values higher than 0.5%, the spread in σ_0^{VV} as a function of increasing surface roughness for the same value of LWC increases, with a reversed trend. Simultaneously increasing LWC eventually generates a σ_0^{VV} increase for all the considered roughness values in this experiment. Interestingly, the higher the surface roughness, the lower LWC value is needed to invert the trend: for $RMSH$ =15 mm (typical of a textured snow surface where suncups are visible, but also very close to the limit of validity of the IEM), σ_0^{VV} starts to increase for $LWC \geq$1%, whereas for $RMSH$ =3 mm, the σ_0^{VV} only starts to increase for $LWC \geq$2%. For LWC values higher than the threshold of 0.5%, the surface roughness influences the C-band backscattering response to an extent that is comparable to the effect of LWC alone over a smooth surface. Similar considerations can be done for the experiments run with the MEMLSv3 permittivity formulation, but as a consequence of the different absorption, the above-mentioned changes in σ_0^{VV} trends happen for lower values of LWC. Besides these considerations, the experiments in Fig. 11 reveal that, regardless of the permittivity formulation, for relatively low values of LWC ($\simeq$1%), a change in surface RMSH from 2 to 3 mm generates a remarkable shift of $\simeq$6 dB in the backscattering response. According to our field observations, such values were typically recorded over snow surfaces undergoing the first cycles of melt-refreeze metamorphism. Interestingly, the value of 6 dB is almost exactly the average bias observed between S1 acquisitions and modeled values of σ_0^{VV} with SMRT during the ripening phase (see Tab. 3). Therefore, we can conclude that the increase in backscattering from the minimum is due to the formation of suncups.

https://doi.org/10.5194/egusphere-2025-974
Preprint. Discussion started: 21 March 2025

5 Discussion

Two consecutive years of detailed snow profiling with a specific focus on the melting season gave an unprecedented overview on the multitemporal evolution of the SAR backscattering as a result of the measured snowpack properties. The identification of the melting phases based on the evolution of multitemporal SAR backscattering as proposed by (Marin et al., 2020) was complicated by two factors: (i) the failure of Sentinel-1B in 2022, which resulted in a halved availability of satellite recordings and (ii) with the ideal incidence angle for wet snow separability being $\simeq 45°$ (Karbou et al., 2021), lower incidence angles likely dampened the backscattering response to wet snow. Despite these limitations, using nothing more than information on σ_0^{VV} change with respect to winter means, the threshold-based method identified the moistening and ripening phases for both years.

Using the first measured time series of surface roughness parameters, we demonstrated that for a high-altitude Alpine snowpack, where radiation can be the dominant energy input during the melting season and surface roughness normally develops several weeks before the snow cover starts forming patches, the observed monotonous increase in backscattering is physically related to the development of surface roughness, from initial surface degradation due to melt-refreeze cycles to the formation of suncups. This connection was only hypothesized by Marin et al. (2020), as without ground data, it is impossible to distinguish the effect of surface roughness from patchy snow using multitemporal SAR backscattering alone. Additionally, the start of the monotonous increase in multitemporal SAR backscattering defines the local minima in the time series. Several studies were carried out in recent years where such minima were associated to the runoff start (Gagliano et al., 2023; Darychuk et al., 2023). However, the proximity of backscatter minimum and runoff start is not due to SAR direct detection of meltwater. Instead, this apparent coincidence arises at the specific frequency of S1 because of an interplay of several factors. As the snowpack reaches the maximum detectable water content by S1 (which reduces scattering), surface roughness begins to develop, enhancing scattering. These mechanisms will be discussed individually in the remaining of this discussion. Based on our data, the only and most likely conclusion we can extrapolate from the backscattering minima from a practical point of view is that the snowpack is in an isothermal state and likely *already* releasing water. However, processes such as melt-refreeze cycles, sublimation, compaction, or settlement in the upper snow layers can potentially lead to the formation of rough surfaces before the snowpack starts releasing meltwater runoff. Therefore, it is relevant to rethink how information on backscattering minima are used for hydrological applications, especially when counting on a limited satellite revisit frequency. Further research should investigate other potential energy input mechanisms that are typical of snowpacks in environments outside the high-altitude and mid-latitude conditions explored in this study.

Reproducing satellite backscattering through radiative transfer modeling driven by field measurements involves accounting for several sources of uncertainty, which can be categorized into two main factors: LWC and surface roughness. The uncertainty associated to LWC manifests itself in many different ways: the time lag between satellite and measurement acquisitions, the scattering originating from surface structures formed by melt-refreeze cycles, the spatial heterogeneity of the LWC distribution, the instrument uncertainty associated to the measurements and, more on the RT modeling side, a lack of a definite permittivity

https://doi.org/10.5194/egusphere-2025-974
Preprint. Discussion started: 21 March 2025

formulation for wet snow. The uncertainty associated to roughness is mostly linked to measurement inaccuracies (and/or not representativeness for the entire S1 cell) and, on the RT modeling side, to possible errors in the IEM surface model.

Within the approximately 5 hours separating satellite and measurements acquisitions, the liquid water per layer can change significantly (Kendra et al., 1998; Techel and Pielmeier, 2011), especially during the moistening and ripening phases or within cold spells, as indicated by the higher simulation variabilities in Fig. 9. Especially on early stages of the melt process, our measurements are likely not representative for the snowpack state overlooked by S1 because of the strong effect of melt-refreeze. Our findings confirm that C-band σ_0^{VV} is highly sensitive to diurnal snowpack variability, particularly during the early stages of melting when features such as melt-refreeze crusts are present (Lund et al., 2022; Brangers et al., 2024). As noted in Brangers et al. (2024), this strong dependence complicates LWC retrievals significantly at these latitudes. This point raises concerns, because the early stages of melting represent a critical period when S1 can detect LWC and likely the only window of opportunity to obtain and integrate reasonable information.

Another issue is the instrument uncertainty in LWC measurements. The deviations between dielectric and calorimetric measurements that we obtained throughout the campaign are in line with previous field and lab studies (Kinar and Pomeroy, 2015; Avanzi et al., 2016). Unexpectedly, co-located measurements in 2023 in the presence of ice lenses showed smaller deviations with respect to simultaneous measurements in 2024. Localized high values of LWC, such as for ponding meltwater above ice lenses, can pose accuracy problems for instruments that empirically estimate the volumetric liquid water content from the snow permittivity (Techel and Pielmeier, 2011). However, as already discussed, their presence could homogenize the overall liquid water distribution among the cell overlooked by the satellite. The increased variability between measurement techniques in 2024 may be (at least partially) due to the increased LWC hetereogeneity compared to 2023. This may indicate that the snowpack stratigraphy and LWC conditions play a larger role than measurement errors due to spatial and temporal offsets. Accounting for the LWC instrument uncertainty, which we estimated to approximately 1% from our data and which are in line with previous similar comparative studies (Techel and Pielmeier, 2011; Donahue et al., 2022), generates an uncertainty range in the simulated σ_0^{VV} which is higher than the variability of the satellite recorded σ_0^{VV} over the course of one snow season. Highest deviations happen for highest values of LWC, in accordance with the findings of Veyssière et al. (2019).

Finally, the lack of a definitive permittivity formulation for wet snow poses a significant challenge for the scientific community. Developing a comprehensive model applicable across all frequencies and LWC conditions is crucial. This study highlights the discrepancies between simulated and actual S1 backscattering measurements, possibly due to overestimated absorption loss in existing models. While matching the observed backscattering would suggest an imaginary permittivity similar to that at 1 GHz, this would imply unrealistic penetration depths at C-band, contradicting field observations (Ulaby and Herschel Stiles, 1981; Shi and Dozier, 1995; Ulaby et al., 2014; Lodigiani et al., 2025). Despite this uncertainty, utilizing two different models derived from distinct mixing theories, yet exhibiting similar spectral shapes (see Fig. 3), allowed for an evaluation of the impact of various uncertainty sources and scattering mechanisms. However, the inherent limitations in wet snow permittivity models prevented a detailed quantitative analysis of individual scattering contributions. This remains an important area for future research.

https://doi.org/10.5194/egusphere-2025-974
Preprint. Discussion started: 21 March 2025

Later in the melting season, the effects of the uncertainties associated to LWC become weaker, because the snowpack surface becomes wetter and the scattering is mostly dominated by surface effects (Shi and Dozier, 1992) – this can be observed in Fig. 9 on dates where the variabilities associated to LWC decrease gradually as a function of time. On these stages, deviations between radiative transfer simulations and satellite acquisitions are mostly explained by inaccuracies in surface roughness measurements. This is clearly demonstrated by cases where there is a notable loss of simulation accuracy following a spring snowfall, after surface roughness had already begun to develop (see "buried roughness" instances in Fig. 9). However, at these later stages of the melting process, simulations reproduce the recorded backscattering generally well. Further deviations can be attributed to the possibility that the panel measurements may not fully capture the roughness observed by the satellite. Additionally, the IEM model, which translates roughness parameters into scattering, could be affected by inaccuracies, particularly when the roughness is high enough to approach the limits of the model's validity (see Fig. 3.2).

In other words, with Fig. 9, we tried to reproduce S1 σ_0^{VV} over a 20 × 20 m cell using physically based averages of fine, detailed snow properties measured at the point scale. At wider scales, the relative importance of very specific information on the state of the snowpack may decrease compared to more influential large-scale scattering drivers, namely the development of internal snowpack structures (e.g. ice lenses and crusts), the soil features in the case of an isothermal but predominantly dry snowpack, and large-scale surface roughness. Although the modularity and comprehensiveness of SMRT theoretically allows most of these scenarios to be modeled, the problem of how to quantify them on a large scale persists.

In Fig. 11, we selected a realistic snowpack layering observed in the field and used the full range of measured values of surface roughness to repeat the experiments done in the past by Shi and Dozier (1992) to characterize the scattering response to increasing surface roughness on a wet snow cover. Since the relationship between co-polarized signals and snow wetness is controlled by the scattering mechanisms, the type of correlation between superficial LWC and surface roughness expresses the relative contribution of volume rather than surface scattering mechanisms (Shi and Dozier, 1992). Shi and Dozier (1992) found negative correlations with surface roughness for LWC between 2 and 4% and a positive correlation with increasing surface wetness at an incidence angle of 50°. Similar results were also found by Ulaby and Herschel Stiles (1981) at frequencies of 8.6 GHz and incidence angles greater than 50°. Our results generally confirm these findings, but the wider range of explored combinations of surface roughness and LWC reveals that the correlation tilt does not occur at a specific LWC value. For RMSH values between 2 and 10 mm, typical of snow during most of the melting period, the tilt depends on both LWC and RMSH, shifting towards higher LWC with lower RMSH. Specifically, backscattering strongly depends on LWC when $RMSH \leq 3$ mm. For low RMSH values (1–2 mm), both permittivity models saturate σ_0^{VV} below -30 dB, a value never recorded by S1, even in multi-year time series, where saturation occurs around -20 dB.

An interesting finding from Fig. 9 is that the most accurate simulations of S1 recordings happen with measured values of surface RMSH above or equal the threshold value of 3 mm. Fig. 11 shows that, for relative low values of LWC between 1 and 1.5%, the backscattering response increases by approximately 6 dB when the roughness RMSH increases from 2 to 3 mm. The value of 6 dB is almost exactly the bias we observed in Fig. 9 between S1 recordings and our simulations, especially with increasing LWC. Similar deviations were found by Veyssière et al. (2019) using MEMLS&a to reproduce σ_0^{VV} during consecutive melt seasons over Alpine areas. Additionally, for LWC values $\geq$1.5% and RMSH between 3 and 4 mm, the simulated

https://doi.org/10.5194/egusphere-2025-974
Preprint. Discussion started: 21 March 2025

σ_0^{VV} saturates at values that are comparable to those recorded by S1. This raises the point that more representative estimates of surface roughness for the entire S1 cell, and/or improved IEM modeling to translate this information into backscattering signals, could be just as crucial as rigorous permittivity formulations for accurately reproducing and better interpreting multi-temporal S1 σ_0^{VV}. Finally, Fig. 11 suggests that with an estimate of the surface LWC from a detailed snow model and recorded values of S1 backscattering, it is in principle possible to give an estimate of the surface roughness. This would inform on two interesting points. On the one hand, based on the position with respect to the curve tilt, it would be possible to have information about the dominance of the volume versus surface scattering mechanism. A prevalence of volume scattering would mean that the snowpack has not yet become a complete black body for C-band radar backscattering. On the other hand, the value of surface roughness could be assimilated in physically based snow models to estimate important metrics for the computation of turbulent heat fluxes, such as the aerodynamic roughness length (Lehning et al., 2011).

Although promising for future research, this paper comes with a number of limitations. LWC is a key variable for interpreting and reproducing S1 acquisitions using radiative transfer models. However, despite ongoing advancements, accurately measuring LWC in the field, modeling it within physically based snow models, and accounting for it into permittivity models remain significant challenges which need to be solved individually. The halved availability of satellite data acquisitions due to the failure of Sentinel-1B in the exact time span when this study was carried out hindered the possibility to obtain more information than those presented on the relationship between melting processes and the multitemporal SAR backscattering. Finally, despite this study enhanced significantly the understanding of the interaction of SAR backscattering with wet snow, these findings are likely valid for high-Alpine regions, i.e. homogeneously covered by a rather high amount of snow, and where surface roughness can develop before the snow cover disappears in patches. However, the launch of the Sentinel-1C satellite will shortly restore the mission's full capabilities, providing enhanced data availability. This development will hopefully spark greater interest in the field, driving research efforts to address the above mentioned limitations, explore mechanisms in environments outside the one explored in this study, and potentially establish a new role for radiative transfer modeling – specifically, to inform physically-based snow models for hydrological applications.

6 Conclusions

In this paper, we presented a unique dataset of wet snow scattering properties collected at a high temporal resolution over two snow seasons at the high-Alpine field site of Weissfluhjoch, Davos, Switzerland. Using this dataset, we analyzed the correlation between melting snow properties and multitemporal SAR backscattering from S1, and reproduced the acquired satellite signals using the radiative-transfer model SMRT. Our data show that the moistening and the ripening phase, being mostly related to the presence of liquid water in the snowpack, are generally well recognized using time series of multitemporal SAR backscattering from S1. The runoff onset, often associated with local minima in multitemporal SAR backscattering, is not detectable by the satellite. With our measurements, we showed that these local minima result from a combination of surface wetting, which reduces backscattering until the S1 signal saturates, and the development of surface roughness before the snow cover begins to disappear in patches, leading to an increase in backscattering. Therefore, it is important to rethink how this information is

https://doi.org/10.5194/egusphere-2025-974
Preprint. Discussion started: 21 March 2025

used for hydrological applications at high elevations and mid-latitudes, especially when counting on reduced satellite revisit times, like in this study. Then, we used our dataset as input to the SMRT model to reproduce the S1 backscattering signal. The simulations were generally affected by a negative bias with respect to the satellite data, with the most significant drivers being LWC in earlier stages of the melt process and the surface roughness later on. Furthermore, we highlighted key difficulties in electromagnetic modeling of melting snowpacks based on field measurements. These challenges include uncertainties primarily deriving from the spatial and temporal variability of LWC between measurements and satellite acquisitions, inaccuracies in surface roughness measurements, and the validity of permittivity and roughness models for wet snow at C-band. Despite these uncertainties, radiative transfer modeling forced by ground measurements allowed in-depth physical interpretations of scattering mechanisms at different melting stages. Specifically, the unprecedented time series of measured surface roughness parameters made it possible to explore and define the scattering effect of roughness over wetting snowpacks. Our findings suggest that accurately quantifying surface roughness and/or improving the transfer function in IEM modeling could be as critical as developing new, rigorous permittivity formulations to enhance S1 retrievals and enhance the understanding of scattering mechanisms on wet snow at these wavelengths. With improved process understanding, the imminent restoration of the the Sentinel mission full capabilities, and further validation efforts in radiative transfer sub-modules, the use of C-band satellite radar signals for snow hydrology applications could proceed further, with radiative transfer models possibly informing physically based snow models.

Code and data availability. The code to reproduce the simulations and plot of Fig. 9 are available on GitHub (https://github.com/carlettif/multitemporal-s1-backscattering). The SMRT model code is available on GitHub (https://github.com/smrt-model/smrt/releases/tag/v1.1). The manually measured and automatically recorded data used in this paper are available on Envidat (https://doi.org/10.16904/envidat.574). All Sentinel-1 data is freely available at https://dataspace.copernicus.eu/ upon registration.

Author contributions. Conceptualization: FC, CM, MB, ML. Data acquisition: MB, FC, CG, CM and all authors listed on EnviDat. Data curation: CG and FC. Methodology: CM and FC. Formal analysis, investigation, visualization: FC. Project administration: MB, CM, ML, FC. Funding acquisition: CM, MB, ML. Writing – original draft: FC. Writing – review and editing: all authors.

Competing interests. The authors declare that they have no competing interests.

Acknowledgements. This research was funded by the Swiss National Science Foundation, grant number 20021-205190. The authors acknowledge all the project partners and employees who took part in the measurement campaign and the contributors to the development of the SMRT model.

https://doi.org/10.5194/egusphere-2025-974
Preprint. Discussion started: 21 March 2025

References

Achammer, T. and Denoth, A.: Snow dielectric properties: from DC to microwave X-band, Annals of Glaciology, 19, 92–96, https://doi.org/10.3189/S0260305500011034, 1994.

Anttila, K., Manninen, T., Karjalainen, T., Lahtinen, P., Riihelä, A., and Siljamo, N.: The temporal and spatial variability in submeter scale surface roughness of seasonal snow in Sodankylä Finnish Lapland in 2009–2010, Journal of Geophysical Research: Atmospheres, 119, 9236–9252, https://doi.org/https://doi.org/10.1002/2014JD021597, 2014.

Avanzi, F., Hirashima, H., Yamaguchi, S., Katsushima, T., and De Michele, C.: Observations of capillary barriers and preferential flow in layered snow during cold laboratory experiments, The Cryosphere, 10, 2013–2026, https://doi.org/10.5194/tc-10-2013-2016, 2016.

Barella, R., Marin, C., Mattia, C., Gianinetto, M., Moranduzzo, T., and Notarnicola, C.: A Low-Cost Portable Automatic System for Snow Surface Roughness Measurements Based on Digital Photography, in: 2021 IEEE International Geoscience and Remote Sensing Symposium IGARSS, pp. 5562–5565, https://doi.org/10.1109/IGARSS47720.2021.9553989, 2021.

Barella, R., Bavay, M., Carletti, F., Ciapponi, N., Premier, V., and Marin, C.: Unlocking the potential of melting calorimetry: a field protocol for liquid water content measurement in snow, The Cryosphere, 18, 5323–5345, https://doi.org/10.5194/tc-18-5323-2024, 2024.

Bartelt, P. and Lehning, M.: A physical SNOWPACK model for the Swiss avalanche warning: Part I: numerical model, Cold Regions Science and Technology, 35, 123–145, https://doi.org/https://doi.org/10.1016/S0165-232X(02)00074-5, 2002.

Bellaire, S., van Herwijnen, A., Mitterer, C., and Schweizer, J.: On forecasting wet-snow avalanche activity using simulated snow cover data, Cold Regions Science and Technology, 144, 28–38, https://doi.org/https://doi.org/10.1016/j.coldregions.2017.09.013, international Snow Science Workshop 2016 Breckenridge, 2017.

Beniston, M. and Stoffel, M.: Rain-on-snow events, floods and climate change in the Alps: Events may increase with warming up to 4°C and decrease thereafter, Science of The Total Environment, 571, 228–236, https://doi.org/https://doi.org/10.1016/j.scitotenv.2016.07.146, 2016.

Beniston, M., Farinotti, D., Stoffel, M., Andreassen, L. M., Coppola, E., Eckert, N., Fantini, A., Giacona, F., Hauck, C., Huss, M., Huwald, H., Lehning, M., López-Moreno, J.-I., Magnusson, J., Marty, C., Morán-Tejéda, E., Morin, S., Naaim, M., Provenzale, A., Rabatel, A., Six, D., Stötter, J., Strasser, U., Terzago, S., and Vincent, C.: The European mountain cryosphere: a review of its current state, trends, and future challenges, The Cryosphere, 12, 759–794, https://doi.org/10.5194/tc-12-759-2018, 2018.

Brangers, I., Marshall, H.-P., De Lannoy, G., Dunmire, D., Mätzler, C., and Lievens, H.: Tower-based C-band radar measurements of an alpine snowpack, The Cryosphere, 18, 3177–3193, https://doi.org/10.5194/tc-18-3177-2024, 2024.

Brogioni, M., Pettinato, S., Macelloni, G., Paloscia, S., Pampaloni, P., Pierdicca, N., and Ticconi, F.: Sensitivity of bistatic scattering to soil moisture and surface roughness of bare soils, International Journal of Remote Sensing, 31, 4227–4255, https://doi.org/10.1080/01431160903232808, 2010.

Conger, S. M. and McClung, D. M.: Comparison of density cutters for snow profile observations, Journal of Glaciology, 55, 163–169, https://doi.org/10.3189/002214309788609038, 2009.

Copernicus: Copernicus data hub, https://scihub.copernicus.eu/.

Darychuk, S. E., Shea, J. M., Menounos, B., Chesnokova, A., Jost, G., and Weber, F.: Snowmelt characterization from optical and synthetic-aperture radar observations in the La Joie Basin, British Columbia, The Cryosphere, 17, 1457–1473, https://doi.org/10.5194/tc-17-1457-2023, 2023.

https://doi.org/10.5194/egusphere-2025-974
Preprint. Discussion started: 21 March 2025

Denoth, A.: Snow dielectric measurements, Advances in Space Research, 9, 233–243, https://doi.org/https://doi.org/10.1016/0273-1177(89)90491-2, 1989.

Denoth, A.: An electronic device for long-term snow wetness recording, Annals of Glaciology, 19, 104–106, https://doi.org/10.3189/S0260305500011058, 1994.

Denoth, A., Foglar, A., Weiland, P., Mätzler, C., Aebischer, H., Tiuri, M., and Sihvola, A.: A comparative study of instruments for measuring the liquid water content of snow, Journal of Applied Physics, 56, 2154–2160, https://doi.org/10.1063/1.334215, 1984.

Dingman, S.: Physical Hydrology, Waveland Press, Incorporated, https://books.google.ch/books?id=hhWojwEACAAJ, 2015.

Donahue, C., Skiles, S. M., and Hammonds, K.: Mapping liquid water content in snow at the millimeter scale: an intercomparison of mixed-phase optical property models using hyperspectral imaging and in situ measurements, The Cryosphere, 16, 43–59, https://doi.org/10.5194/tc-16-43-2022, 2022.

Endrizzi, S., Gruber, S., Dall'Amico, M., and Rigon, R.: GEOtop 2.0: simulating the combined energy and water balance at and below the land surface accounting for soil freezing, snow cover and terrain effects, Geoscientific Model Development, 7, 2831–2857, https://doi.org/10.5194/gmd-7-2831-2014, 2014.

Fassnacht, S., Williams, M., and Corrao, M.: Changes in the surface roughness of snow from millimetre to metre scales, Ecological Complexity, 6, 221–229, https://doi.org/https://doi.org/10.1016/j.ecocom.2009.05.003, special Section: Fractal Modeling and Scaling in Natural Systems, 2009.

Fierz, C.: The International Classification for Seasonal Snow on the Ground, IHP-VI Technical Documents in hydrology, UNESCO/IHP, https://books.google.ch/books?id=1Su5ZwEACAAJ, 2009.

Fierz, C. and Föhn, P. M. B.: Long-Term Observation of the Water Content of an Alpine Snowpack, https://api.semanticscholar.org/CorpusID:127054238, 1994.

FPGA Company: SLF InfraSnow Sensor, https://fpga-company.com/wp-content/uploads/2023/01/InfraSnow-User-Manual-Version-1.01.pdf.

Fromm, R., Baumgärtner, S., Leitinger, G., Tasser, E., and Höller, P.: Determining the drivers for snow gliding, Natural Hazards and Earth System Sciences, 18, 1891–1903, https://doi.org/10.5194/nhess-18-1891-2018, 2018.

Fung, A., Li, Z., and Chen, K.: Backscattering from a randomly rough dielectric surface, IEEE Transactions on Geoscience and Remote Sensing, 30, 356–369, https://doi.org/10.1109/36.134085, 1992.

Gagliano, E., Shean, D., Henderson, S., and Vanderwilt, S.: Capturing the Onset of Mountain Snowmelt Runoff Using Satellite Synthetic Aperture Radar, Geophysical Research Letters, 50, e2023GL105 303, https://doi.org/https://doi.org/10.1029/2023GL105303, e2023GL105303 2023GL105303, 2023.

Gergely, M., Wolfsperger, F., and Schneebeli, M.: Simulation and Validation of the InfraSnow: An Instrument to Measure Snow Optically Equivalent Grain Size, IEEE Transactions on Geoscience and Remote Sensing, 52, 4236–4247, https://doi.org/10.1109/TGRS.2013.2280502, 2014.

Günther, D., Marke, T., Essery, R., and Strasser, U.: Uncertainties in Snowpack Simulations—Assessing the Impact of Model Structure, Parameter Choice, and Forcing Data Error on Point-Scale Energy Balance Snow Model Performance, Water Resources Research, 55, 2779–2800, https://doi.org/https://doi.org/10.1029/2018WR023403, 2019.

Hallikainen, M., Ulaby, F., and Abdelrazik, M.: Dielectric properties of snow in the 3 to 37 GHz range, IEEE Transactions on Antennas and Propagation, 34, 1329–1340, https://doi.org/10.1109/TAP.1986.1143757, 1986.

HannaInstrumentsInc.: HI98501 (Checktemp®) Instruction Manual, Hanna Instruments.

https://doi.org/10.5194/egusphere-2025-974
Preprint. Discussion started: 21 March 2025

Husman, S. d. R., Hu, Z., Wouters, B., Munneke, P. K., Veldhuijsen, S., and Lhermitte, S.: Remote Sensing of Surface Melt on Antarctica: Opportunities and Challenges, IEEE Journal of Selected Topics in Applied Earth Observations and Remote Sensing, 16, 2462–2480, https://doi.org/10.1109/JSTARS.2022.3216953, 2023.

Karbou, F., Veyssière, G., Coleou, C., Dufour, A., Gouttevin, I., Durand, P., Gascoin, S., and Grizonnet, M.: Monitoring Wet Snow Over an Alpine Region Using Sentinel-1 Observations, Remote Sensing, 13, https://doi.org/10.3390/rs13030381, 2021.

Kattelmann, R. and Dozier, J.: Observations of snowpack ripening in the Sierra Nevada, California, U.S.A., Journal of Glaciology, 45, 409–416, https://doi.org/10.3189/S002214300000126X, 1999.

Kawashima, K., Endo, T., and Takeuchi, Y.: A portable calorimeter for measuring liquid-water content of wet snow, Annals of Glaciology, 26, 103–106, https://doi.org/10.3189/1998AoG26-1-103-106, 1998.

Kendra, J., Sarabandi, K., and Ulaby, F.: Radar measurements of snow: Experiment and analysis, Geoscience and Remote Sensing, IEEE Transactions on, 36, 864 – 879, https://doi.org/10.1109/36.673679, 1998.

Kinar, N. J. and Pomeroy, J. W.: Measurement of the physical properties of the snowpack, Reviews of Geophysics, 53, 481–544, https://doi.org/https://doi.org/10.1002/2015RG000481, 2015.

Koch, F., Prasch, M., Schmid, L., Schweizer, J., and Mauser, W.: Measuring Snow Liquid Water Content with Low-Cost GPS Receivers, Sensors, 14, 20 975–20 999, https://doi.org/10.3390/s141120975, 2014.

Leduc-Leballeur, M., Picard, G., Mialon, A., Arnaud, L., Lefebvre, E., Possenti, P., and Kerr, Y.: Modeling L-Band Brightness Temperature at Dome C in Antarctica and Comparison With SMOS Observations, IEEE Transactions on Geoscience and Remote Sensing, 53, 4022–4032, https://doi.org/10.1109/TGRS.2015.2388790, 2015.

Lehning, M., Völksch, I., Gustafsson, D., Nguyen, T. A., Stähli, M., and Zappa, M.: ALPINE3D: a detailed model of mountain surface processes and its application to snow hydrology, Hydrological Processes, 20, 2111–2128, https://doi.org/https://doi.org/10.1002/hyp.6204, 2006.

Lehning, M., Grünewald, T., and Schirmer, M.: Mountain snow distribution governed by an altitudinal gradient and terrain roughness, Geophysical Research Letters, 38, https://doi.org/https://doi.org/10.1029/2011GL048927, 2011.

Lin, C.-C., Rommen, B., Floury, N., Schüttemeyer, D., Davidson, M. W. J., Kern, M., Kontu, A., Lemmetyinen, J., Pulliainen, J., Wiesmann, A., Werner, C. L., Mätzler, C., Schneebeli, M., Proksch, M., and Nagler, T.: Active Microwave Scattering Signature of Snowpack—Continuous Multiyear SnowScat Observation Experiments, IEEE Journal of Selected Topics in Applied Earth Observations and Remote Sensing, 9, 3849–3869, https://doi.org/10.1109/JSTARS.2016.2560168, 2016.

Lodigiani, M., Marin, C., and Pasian, M.: Mixed Analytical-Numerical Modeling of Radar Backscattering for Seasonal Snowpacks, IEEE Journal of Selected Topics in Applied Earth Observations and Remote Sensing, 18, 3461–3471, https://doi.org/10.1109/JSTARS.2024.3521612, 2025.

Lombardo, M., Fees, A., Udke, A., Meusburger, K., van Herwijnen, A., Schweizer, J., and Lehmann, P.: Capillary suction across the soil-snow interface as a mechanism for the formation of wet basal layers under gliding snowpacks, Journal of Glaciology, p. 1–46, https://doi.org/10.1017/jog.2025.2, 2025.

Lund, J., Forster, R. R., Deeb, E. J., Liston, G. E., Skiles, S. M., and Marshall, H.-P.: Interpreting Sentinel-1 SAR Backscatter Signals of Snowpack Surface Melt/Freeze, Warming, and Ripening, through Field Measurements and Physically-Based SnowModel, Remote Sensing, 14, https://doi.org/10.3390/rs14164002, 2022.

Lundberg, A., G. N. G. D.: "Ground Trut" snow measurements – review of operational and new measurement methods for Sweden, Norway, and Finland, pp. 215–237, 2008.

https://doi.org/10.5194/egusphere-2025-974
Preprint. Discussion started: 21 March 2025

Magagi, R. and Bernier, M.: Optimal conditions for wet snow detection using RADARSAT SAR data, Remote Sensing of Environment, 84, 221–233, https://doi.org/https://doi.org/10.1016/S0034-4257(02)00104-9, 2003.

Manninen, T., Anttila, K., Karjalainen, T., and Lahtinen, P.: Automatic snow surface roughness estimation using digital photos, Journal of Glaciology, 58, 993–1007, https://doi.org/10.3189/2012JoG11J144, 2012.

Marin, C., Bertoldi, G., Premier, V., Callegari, M., Brida, C., Hürkamp, K., Tschiersch, J., Zebisch, M., and Notarnicola, C.: Use of Sentinel-1 radar observations to evaluate snowmelt dynamics in alpine regions, The Cryosphere, 14, 935–956, https://doi.org/10.5194/tc-14-935-2020, 2020.

Marty, C. and Meister, R.: Long-term snow and weather observations at Weissfluhjoch and its relation to other high-altitude observatories in the Alps, Theoretical and Applied Climatology, 110, https://doi.org/10.1007/s00704-012-0584-3, 2012.

Meloche, J., Langlois, A., Rutter, N., Royer, A., King, J., Walker, B., Marsh, P., and Wilcox, E. J.: Characterizing tundra snow sub-pixel variability to improve brightness temperature estimation in satellite SWE retrievals, The Cryosphere, 16, 87–101, https://doi.org/10.5194/tc-16-87-2022, 2022.

Meloche, J., Leroux, N. R., Montpetit, B., Vionnet, V., and Derksen, C.: Radar Equivalent Snowpack: reducing the number of snow layers while retaining its microwave properties and bulk snow mass, EGUsphere, 2024, 1–18, https://doi.org/10.5194/egusphere-2024-3169, 2024.

Mitchell, K. A. and Tiedje, T.: Growth and fluctuations of suncups on alpine snowpacks, Journal of Geophysical Research: Earth Surface, 115, https://doi.org/https://doi.org/10.1029/2010JF001724, 2010.

Moldestad, D. A.: Characterisation of liquid water content and snow density in a cross-country race ski track, Bulletin of glaciological research, 22, 39–49, 2005.

Murfitt, J., Duguay, C., Picard, G., and Lemmetyinen, J.: Forward modelling of synthetic-aperture radar (SAR) backscatter during lake ice melt conditions using the Snow Microwave Radiative Transfer (SMRT) model, The Cryosphere, 18, 869–888, https://doi.org/10.5194/tc-18-869-2024, 2024.

Mätzler, C.: Applications of the interaction of microwaves with the natural snow cover, Remote Sensing Reviews, 2, 259–387, https://doi.org/10.1080/02757258709532086, 1987.

Naderpour, R., Schwank, M., Houtz, D., Werner, C., and Mätzler, C.: Wideband Backscattering From Alpine Snow Cover: A Full-Season Study, IEEE Transactions on Geoscience and Remote Sensing, 60, 1–15, https://doi.org/10.1109/TGRS.2021.3112772, 2022.

Nagler, T. and Rott, H.: Retrieval of wet snow by means of multitemporal SAR data, IEEE Transactions on Geoscience and Remote Sensing, 38, 754–765, https://doi.org/10.1109/36.842004, 2000.

Nagler, T., Rott, H., Ripper, E., Bippus, G., and Hetzenecker, M.: Advancements for Snowmelt Monitoring by Means of Sentinel-1 SAR, Remote Sensing, 8, https://doi.org/10.3390/rs8040348, 2016.

Perla, R. and Banner, J.: Calibration of capacitive cells for measuring water in snow, Cold Regions Science and Technology, 15, 225–231, https://doi.org/https://doi.org/10.1016/0165-232X(88)90069-9, 1988.

Pfeffer, W. T. and Humphrey, N. F.: Formation of ice layers by infiltration and refreezing of meltwater, Annals of Glaciology, 26, 83–91, https://doi.org/10.3189/1998AoG26-1-83-91, 1998.

Picard, G., Sandells, M., and Löwe, H.: SMRT: an active–passive microwave radiative transfer model for snow with multiple microstructure and scattering formulations (v1.0), Geoscientific Model Development, 11, 2763–2788, https://doi.org/10.5194/gmd-11-2763-2018, 2018.

Picard, G., Leduc-Leballeur, M., Banwell, A. F., Brucker, L., and Macelloni, G.: The sensitivity of satellite microwave observations to liquid water in the Antarctic snowpack, The Cryosphere, 16, 5061–5083, https://doi.org/10.5194/tc-16-5061-2022, 2022a.

https://doi.org/10.5194/egusphere-2025-974
Preprint. Discussion started: 21 March 2025

Picard, G., Löwe, H., and Mätzler, C.: Brief communication: A continuous formulation of microwave scattering from fresh snow to bubbly ice from first principles, The Cryosphere, 16, 3861–3866, https://doi.org/10.5194/tc-16-3861-2022, 2022b.

Picard, G., Löwe, H., Domine, F., Arnaud, L., Larue, F., Favier, V., Le Meur, E., Lefebvre, E., Savarino, J., and Royer, A.: The Microwave Snow Grain Size: A New Concept to Predict Satellite Observations Over Snow-Covered Regions, AGU Advances, 3, e2021AV000 630, https://doi.org/https://doi.org/10.1029/2021AV000630, e2021AV000630 2021AV000630, 2022c.

Porod, G.: Die Röntgenkleinwinkelstreuung von dichtgepackten kolloiden Systemen, Kolloid-Zeitschrift, 124, 83–114, https://doi.org/10.1007/BF01512792, 1951.

Post, A. and LaChapelle, E. R.: Glacier ice, University of Toronto Press, 2000.

Proksch, M., Mätzler, C., Wiesmann, A., Lemmetyinen, J., Schwank, M., Löwe, H., and Schneebeli, M.: MEMLS3a: Microwave Emission Model of Layered Snowpacks adapted to include backscattering, Geoscientific Model Development, 8, 2611–2626, https://doi.org/10.5194/gmd-8-2611-2015, 2015.

Proksch, M., Rutter, N., Fierz, C., and Schneebeli, M.: Intercomparison of snow density measurements: bias, precision, and vertical resolution, The Cryosphere, 10, 371–384, https://doi.org/10.5194/tc-10-371-2016, 2016.

Quéno, L., Vionnet, V., Cabot, F., Vrécourt, D., and Dombrowski-Etchevers, I.: Forecasting and modelling ice layer formation on the snowpack due to freezing precipitation in the Pyrenees, Cold Regions Science and Technology, 146, 19–31, https://doi.org/https://doi.org/10.1016/j.coldregions.2017.11.007, 2018.

Raleigh, M. S., Lundquist, J. D., and Clark, M. P.: Exploring the impact of forcing error characteristics on physically based snow simulations within a global sensitivity analysis framework, Hydrology and Earth System Sciences, 19, 3153–3179, https://doi.org/10.5194/hess-19-3153-2015, 2015.

Rott, H., Scheiblauer, S., Wuite, J., Krieger, L., Floricioiu, D., Rizzoli, P., Libert, L., and Nagler, T.: Penetration of interferometric radar signals in Antarctic snow, The Cryosphere, 15, 4399–4419, https://doi.org/10.5194/tc-15-4399-2021, 2021.

Sandells, M., Löwe, H., Picard, G., Dumont, M., Essery, R., Floury, N., Kontu, A., Lemmetyinen, J., Maslanka, W., Morin, S., Wiesmann, A., and Mätzler, C.: X-Ray Tomography-Based Microstructure Representation in the Snow Microwave Radiative Transfer Model, IEEE Transactions on Geoscience and Remote Sensing, 60, 1–15, https://doi.org/10.1109/TGRS.2021.3086412, 2022.

Schmid, L., Heilig, A., Mitterer, C., Schweizer, J., Maurer, H., Okorn, R., and Eisen, O.: Continuous snowpack monitoring using upward-looking ground-penetrating radar technology, Journal of Glaciology, 60, 509–525, https://doi.org/10.3189/2014JoG13J084, 2014.

Shi, J. and Dozier, J.: Radar Backscattering Response to Wet Snow, in: [Proceedings] IGARSS '92 International Geoscience and Remote Sensing Symposium, vol. 2, pp. 927–929, https://doi.org/10.1109/IGARSS.1992.578299, 1992.

Shi, J. and Dozier, J.: Inferring snow wetness using C-band data from SIR-C's polarimetric synthetic aperture radar, IEEE Transactions on Geoscience and Remote Sensing, 33, 905–914, https://doi.org/10.1109/36.406676, 1995.

Shi, J., Dozier, J., and Rott, H.: Deriving snow liquid water content using C-band polarimetric SAR, in: Proceedings of IGARSS '93 - IEEE International Geoscience and Remote Sensing Symposium, pp. 1038–1041 vol.3, https://doi.org/10.1109/IGARSS.1993.322643, 1993.

Sihvola, A. H. and Tiuri, M. E.: Snow Fork for Field Determination of the Density and Wetness Profiles of a Snow Pack, IEEE Transactions on Geoscience and Remote Sensing, GE-24, 717–721, https://api.semanticscholar.org/CorpusID:10134466, 1986.

Smith, C. D., Kontu, A., Laffin, R., and Pomeroy, J. W.: An assessment of two automated snow water equivalent instruments during the WMO Solid Precipitation Intercomparison Experiment, The Cryosphere, 11, 101–116, https://doi.org/10.5194/tc-11-101-2017, 2017.

https://doi.org/10.5194/egusphere-2025-974
Preprint. Discussion started: 21 March 2025

Soriot, C., Picard, G., Prigent, C., Frappart, F., and Domine, F.: Year-round sea ice and snow characterization from combined passive and active microwave observations and radiative transfer modeling, Remote Sensing of Environment, 278, 113 061, https://doi.org/https://doi.org/10.1016/j.rse.2022.113061, 2022.

Strozzi, T., Wiesmann, A., and Mätzler, C.: Active microwave signatures of snow covers at 5.3 and 35 GHz, Radio Science, 32, 479–495, https://doi.org/10.1029/96RS03777, 1997.

Techel, F. and Pielmeier, C.: Point observations of liquid water content in wet snow ndash; investigating methodical, spatial and temporal aspects, The Cryosphere, 5, 405–418, https://doi.org/10.5194/tc-5-405-2011, 2011.

Ulaby, F., Long, D., Blackwell, W., Elachi, C., Fung, A., Ruf, C., Sarabandi, K., Zyl, J., and Zebker, H.: Microwave Radar and Radiometric Remote Sensing, 2014.

Ulaby, F. T. and Herschel Stiles, W.: Microwave response of snow, Advances in Space Research, 1, 131–149, https://doi.org/https://doi.org/10.1016/0273-1177(81)90389-6, 1981.

Ulaby, F. T., Moore, R. K., and K., F. A.: Microwave Remote Sensing. Active and Passive. Vol. 3. From Theory to Applications, x + pp. 1065–2162. Norwood, MA: Artech House Inc. Price £79.00. ISBN 0 89006 192 0., Geological Magazine, 124, 88–88, https://doi.org/10.1017/S0016756800015831, 1987.

Veyssière, G., Karbou, F., Morin, S., Lafaysse, M., and Vionnet, V.: Evaluation of Sub-Kilometric Numerical Simulations of C-Band Radar Backscatter over the French Alps against Sentinel-1 Observations, Remote Sensing, 11, https://doi.org/10.3390/rs11010008, 2019.

Viviroli, D. and Weingartner, R.: The hydrological significance of mountains: from regional to global scale, Hydrology and Earth System Sciences, 8, 1017–1030, https://doi.org/10.5194/hess-8-1017-2004, 2004.

Wever, N., Würzer, S., Fierz, C., and Lehning, M.: Simulating ice layer formation under the presence of preferential flow in layered snowpacks, The Cryosphere, 10, 2731–2744, https://doi.org/10.5194/tc-10-2731-2016, 2016.

Williams, L. D. and Gallagher, J. G.: The Relation of Millimeter-Wavelength Backscatter to Surface Snow Properties, IEEE Transactions on Geoscience and Remote Sensing, GE-25, 188–194, https://doi.org/10.1109/TGRS.1987.289817, 1987.

Wolfsperger, F., Ziegler, S., Schneebeli, M., and Löwe, H.: Evaluation of the InfraSnow: a handheld device to measure snow specific surface (SSA), https://doi.org/10.13140/RG.2.2.31566.95047, 2022.

Wolfsperger, F., Geisser, M., Ziegler, S., and Löwe, H.: A NEW HANDHELD CAPACITIVE SENSOR TO MEASURE SNOW DENSITY AND LIQUID WATER CONTENT, 2023.

Würzer, S., Jonas, T., Wever, N., and Lehning, M.: Influence of Initial Snowpack Properties on Runoff Formation during Rain-on-Snow Events, Journal of Hydrometeorology, 17, 1801 – 1815, https://doi.org/10.1175/JHM-D-15-0181.1, 2016.

Yueh, S. H., Dinardo, S. J., Akgiray, A., West, R., Cline, D. W., and Elder, K.: Airborne Ku-Band Polarimetric Radar Remote Sensing of Terrestrial Snow Cover, IEEE Transactions on Geoscience and Remote Sensing, 47, 3347–3364, https://doi.org/10.1109/TGRS.2009.2022945, 2009.

Zuanon, N.: IceCube, a portable and reliable instrument for snow specific surface area measurement in the field, https://api.semanticscholar.org/CorpusID:128982547, 2013.

Appendix A

https://doi.org/10.5194/egusphere-2025-974
Preprint. Discussion started: 21 March 2025

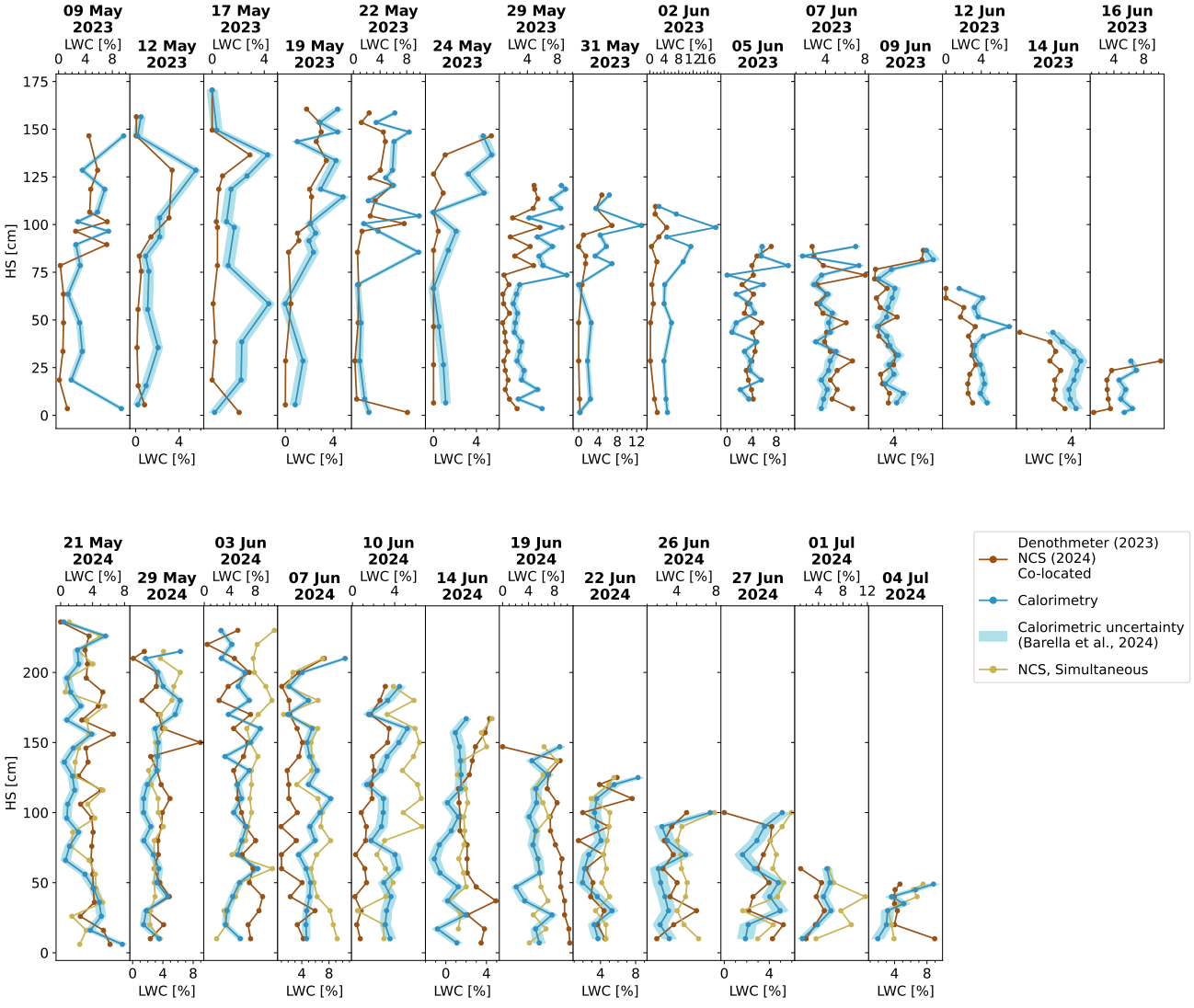

Figure A1. Direct comparison of measured profiles of liquid water content with dielectric methods (brown) and melting calorimetry (blue). The uncertainty associated with melting calorimetry measurements as of Barella et al. (2021) is shown by means of the light blue shaded area. In 2024, a second profile using dielectric instruments (yellow) was simultaneously carried out alongside the melting calorimetry.

https://doi.org/10.5194/egusphere-2025-974
Preprint. Discussion started: 21 March 2025

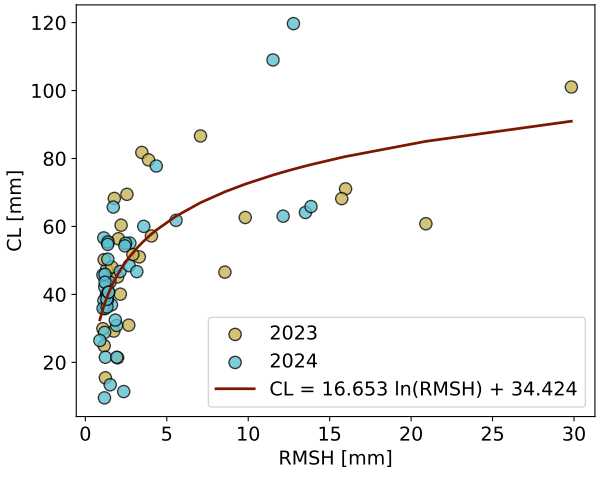

Figure A2. Empirical logarithmic relationship fitted on field data between the surface roughness parameters of RMSH and CL, based on a total of N=75 values over the measurement campaigns of 2023 (yellow) and 2024 (light blue).